

PREPARED FOR SUBMISSION TO

Probing Light Dark Particles in Neutrino Scattering Experiments

Ruofei Feng¹, Shao-Feng Ge^{2,3}, Yongchao Zhang^{1,4}

¹*School of Physics, Southeast University, Nanjing 211189, China*

²*State Key Laboratory of Dark Matter Physics, Tsung-Dao Lee Institute & School of Physics and Astronomy, Shanghai Jiao Tong University, China*

³*Key Laboratory for Particle Astrophysics and Cosmology (MOE) & Shanghai Key Laboratory for Particle Physics and Cosmology, Shanghai Jiao Tong University, Shanghai 200240, China*

⁴*Center for High Energy Physics, Peking University, Beijing 100871, China*

E-mail: fengrf@seu.edu.cn, gesf@sjtu.edu.cn,
zhangyongchao@seu.edu.cn

ABSTRACT: In this work we investigate the production of a dark fermionic particle χ in the neutrino scattering experiments. In the framework of effective field theory, such process can be induced by the effective four-fermion interactions involving neutrinos, the dark particle χ and standard model particles. In particular, we examine the constraints on the effective couplings from the neutrinos scattering off nuclei in the COHERENT and CONUS+ experiments as well as the prospects at the DUNE near detector from neutrino-electron scattering. It turns out the current COHERENT and CONUS+ constraints on the cutoff scales are less stringent than those from the existing Large Hadron Collider data. However, the DUNE near detector could probe the cutoff scales beyond the existing CHARM II and LEP limits up to roughly 1 TeV, for the dark particle mass up to roughly 50 MeV.

Contents

| | | |
|----------|--|-----------|
| 1 | Introduction | 1 |
| 2 | Neutrino scattering into a dark particle | 4 |
| 2.1 | EFT setup | 4 |
| 2.2 | Dark particle decay | 7 |
| 2.3 | Kinematic analysis | 8 |
| 3 | Analysis details | 10 |
| 3.1 | COHERENT | 10 |
| 3.2 | CONUS+ | 13 |
| 3.3 | DUNE Near Detector | 15 |
| 4 | Hadronic absorption operators | 17 |
| 4.1 | Exclusion limits from COHERENT and CONUS+ | 17 |
| 4.2 | Limits from LHC data, FCNC meson decays and SN1987A | 20 |
| 4.3 | Other weak constraints | 22 |
| 5 | Leptonic absorption operators | 22 |
| 5.1 | The sensitivities at DUNE ND | 23 |
| 5.2 | CHARM II and LEP limits and prospects at future lepton colliders | 25 |
| 5.3 | Other weak constraints | 26 |
| 6 | Conclusion | 28 |
| A | Weak nuclear form factor and spin structure functions | 28 |
| B | Nucleon form factors | 29 |

1 Introduction

With the very recent updates of neutrino oscillation data by the JUNO experiment [1], we have entered the precision neutrino physics era at the sub-percentage level. However, neutrinos are still the most mysterious particles in the standard model (SM). For instance, we do not know much about the nature of neutrinos (Dirac or Majorana particles), the origin of their tiny masses, or whether there are extra heavier states, etc [2]. On the other hand, after decades of efforts, dark matter (DM) has not been undoubtedly confirmed in any of the direct detection, indirect detection or high-energy collider searches, in spite of the various astrophysical and cosmological evidence [3–6]. Besides DM, there could exist a hidden sector of dark particles to be explored. Therefore, the new physics (NP) beyond

the SM of particle physics is essential for understanding the basic properties of neutrinos and dark particles, as well as other open questions in the SM.

Although both neutrinos and the dark particle χ are always “invisible” particles in the laboratory experiments and astrophysical observations, they could potentially interact sizably with each other (and the SM particles); see Ref. [7] for a recent comprehensive study. In the framework of effective field theory (EFT), there might exist the interactions of neutrinos ν and dark fermion χ with SM quarks or charged leptons $f = q, \ell$, in the form of effective four-fermion absorption operators of

$$\mathcal{O}_i \equiv (\bar{\chi} \Gamma^i P_L \nu)(\bar{f} \Gamma_i f), \quad (1.1)$$

where $P_L \equiv (1 - \gamma^5)/2$ is the left-handed projector, and Γ_i stands for different Lorentz structures. Such effective couplings can originate from the simplified models with heavy mediators [8, 9]. These EFT operators can induce very rich phenomenological signals. Depending on the underlying processes involved, the phenomenological implications can be classified into the following categories (for the sake of cleanliness, the charge conjugate processes are not explicitly shown, e.g. $f\bar{f} \rightarrow \nu\bar{\chi}$ implies also the process $f\bar{f} \rightarrow \chi\bar{\nu}$ by charge conjugation).

- The decay of χ . The most immediate implication of the operator in Eq. (1.1) is the decay of the dark fermion χ at the tree-level $\chi \rightarrow \nu f\bar{f}$ or at the 1-loop order $\chi \rightarrow \nu\gamma, \nu\gamma\gamma, \nu\gamma\gamma\gamma$ [10, 11]. To stabilize a decaying DM at the cosmological scale, there are some requirements on the the mass m_χ and couplings relevant, depending on the decay channels. However, our current study does not rely on the dark fermion χ to be a DM candidate but takes it as a dark sector particle for generality.
- $f^{(*)} + \bar{f}^{(*)} \rightarrow \nu + \bar{\chi}$. At high-energy hadron colliders, f is the parton quarks involved, and neutrinos and the dark particle χ can be pair produced and behave as missing transverse energy \cancel{E}_T . The dominant search channels are the mono-jet, mono- γ and mono- Z/W processes [12–14], which are very similar to the signals of dark particles at hadron colliders [15–17]. At lepton colliders, f denotes the charged leptons, and the most promising signals are mono- γ and $e^+e^- + \cancel{E}_T$ processes [18]. There have been very extensive studies of dark particles at the lepton colliders [17, 19–35] and from (semi-)invisible meson decays [25, 36–50]. At the 1-loop order, the operator induces the exotic invisible decay mode $Z \rightarrow \nu\bar{\chi}$, with f and \bar{f} being virtual particles in the loop [51].
- $f^* \rightarrow f^{(*)} + \nu + \bar{\chi}$. Here f^* stands for off-shell SM particles, e.g. internal quark or charged lepton lines. For instance, the operators could induce the rare meson decay $M^- \rightarrow \ell^-\nu\nu\bar{\chi}$ and the exotic W boson decay $W \rightarrow \ell\nu\nu\bar{\chi}$. Such processes are quite similar to the neutrino self-interaction induced processes $M^- \rightarrow \ell^-\nu\nu\bar{\nu}$ and $W \rightarrow \ell\nu\nu\bar{\nu}$ [52–55]. If dark particle is involved, the pair production of dark particles in the fixed-target experiments are also of this category [17, 31, 32, 46, 47, 56–66]. The couplings of neutrino and dark particle χ with up-type quarks will contribute at the 1-loop order to the flavor-changing neutral current (FCNC) processes $d_j \rightarrow d_i \nu\bar{\chi}$

(with $d_{i,j}$ the down-type quarks and i, j the generation indices), which have the same experimental signals as the SM FCNC process $d_j \rightarrow d_i \nu \bar{\nu}$ (including the extra contribution from neutrino non-standard interactions (NSIs) [67]) and the DM pair production in FCNC meson decay $d_j \rightarrow d_i \chi \bar{\chi}$ [37, 40, 45, 63, 68–70]. There are also recently some studies on the dark particle pair production from the flavor-conserving meson decay $\eta \rightarrow \pi^0 \chi \bar{\chi}$ [71–76].

- $\nu^* \rightarrow \chi + f + \bar{f}$. Here ν^* is an off-shell neutrino, e.g. from SM particle decays. The typical processes of this category are the four-body meson decay $M^- \rightarrow \ell^- \bar{\chi} \ell'^+ \ell'^-$, four-body tauon decay $\tau^- \rightarrow \pi^- \chi \ell^+ \ell^-$ and five-body charged lepton decay $\ell_\gamma^- \rightarrow \ell_\alpha^- \ell_\beta^+ \ell_\beta^- \nu \bar{\chi}$. At the 1-loop order, the operator in Eq. (1.1) could induce the exotic tauon decay $\tau^- \rightarrow \pi^- \chi$ [51].
- $\chi + f \rightarrow \nu + f$. In DM direct detection experiments and low threshold neutrino experiments, the effective operator in Eq. (1.1) could induce the absorption of DM and convert all its mass into the kinematic energy [9, 12–14, 77, 78]. Such a mechanism could significantly enhance the recoil energy in DM direct detection experiments, and as a result suitable for the searches of relatively light DM particles. High energy neutrinos can be produced from the scattering of relatively heavy DM with SM particles in the Sun or the Earth [78].
- $\nu^{(*)} + f^{(*)} \rightarrow \chi + f$. The dark fermion χ can be produced in neutrino scattering experiments.¹ The signal is the recoil energy of the target nuclei or electrons, as in DM direct detection experiments [9, 78, 80]. Such a process can also occur in the supernova core, which then leads to extra energy loss mechanisms and is thus constrained by the observations of SN1987A [81]. The operator could also induce the exotic radiative decays of charged mesons $M^- \rightarrow \ell^- \bar{\chi}$ and W boson $W^- \rightarrow \ell^- \bar{\chi}$ [51].

In this paper, we take a general case for the fermion χ in the dimension-6 operator (1.1) to be a dark particle, e.g. some non-DM components in the dark sector. The fermion χ could also be a heavy sterile neutrino, e.g. from the type-I seesaw [82–86]. Generally speaking, the signals of the dark particle χ are quite similar to the DM case. However, there are still some differences: (i) The lifetime constraints on the dark particle χ is relaxed a lot, with respect to the DM case [10, 11]. (ii) The DM absorption process $\chi + f \rightarrow \nu + f$ at DM direct detection experiments applies only to the searches of stable DM particles (at the cosmological time scale), but not to the dark particle χ that needs not to be stable.

We explore the production of dark particle χ from the scattering of neutrinos with the target nuclei in the experiments COHERENT, CONUS+, and with electrons in the DUNE near detector (ND), originating from the operators in Eq. (1.1) with all the possible Lorentz structures. There have been some relevant studies in the literature in the framework of effective operators [8, 9], or in the simplified model with mediators [80, 87–89]. If χ is identified as a heavy sterile neutrino, it can be produced from the heavy-light

¹A recent comprehensive EFT analysis of the coherent elastic neutrino-nucleus scattering (CE ν NS) can be found in Ref. [79].

neutrino mixing [90–95] (see Refs. [96, 97] for comprehensive lists of limits on heavy-light neutrino mixings) or from the neutrino magnetic moments [98–109]. It turns out that the constraints of the current COHERENT and CONUS+ data on the cutoff scales for the effective couplings could only go up to ~ 700 GeV at the 90% confidence level (C.L.), much weaker than those limits from the current Large Hadron Collider (LHC) data, up to ~ 11 TeV [13] (cf. Fig. 5 and Table 1). In contrast, the cutoff scales for the couplings involving electrons could be probed up to ~ 1 TeV at the 90% C.L. at DUNE ND, beyond the existing CHARM II and LEP limits [9, 20]. The sensitivities can be further improved up to tens of TeV at future high-energy lepton colliders [18], such as the Future Circular Collider (FCC-ee) [110], Circular Electron-Positron Collider (CEPC) [111], International Linear Collider (ILC) [112, 113] and Compact Linear Collider (CLIC) [114] (cf. Fig. 6 and Table 2).

The rest of this paper is organized as follows. The EFT setup is sketched in Sec. 2, including some details on the decay of χ and the basic kinematic analysis. The full analysis details for the constraints of COHERENT and CONUS+ and the sensitivities of DUNE ND are presented in Sec. 3. The probe of hadronic absorption operators at COHERENT and CONUS+ are detailed in Sec. 4 while the DUNE ND sensitivities on the leptonic operators are obtained in Sec. 5. In these two sections, we also compare our results to the main existing constraints and future prospects, and collect the relevant weaker constraints. We conclude in Sec. 6. For the convenience of readers, the weak nuclear form factors and spin structure functions for the calculations in Sec. 2.1 are collected in Appendix A; the nucleon form factors are listed in Appendix B, which are relevant to the content in Sec. 4.2.

2 Neutrino scattering into a dark particle

2.1 EFT setup

In the framework of EFT, the coupling of neutrinos ν_α of flavor $\alpha = e, \mu, \tau$ with the dark fermion χ and the target fermion f (electron e or nucleon N) can be written as

$$\mathcal{L}_{\text{eff}} = \sum_{i,f} \frac{\mathcal{O}_i}{\Lambda_{i,f}^2} + \text{h.c.}, \quad (2.1)$$

where $f = e, N$, and the index i runs over all the five possible Lorentz structures for the new interactions: scalar (S), pseudo-scalar (P), vector (V), axial-vector (A) or tensor (T). These Lorentz structures correspond to the matrices of $\Gamma^i \equiv \{I, i\gamma^5, \gamma^\mu, \gamma^\mu\gamma^5, \sigma^{\mu\nu}\}$, respectively, with $\sigma^{\mu\nu} \equiv \frac{i}{2}[\gamma^\mu, \gamma^\nu]$. The parameter $\Lambda_{i,f}$ is an effective cutoff scale that characterizes the strength of the interaction: a smaller $\Lambda_{i,f}$ implies a stronger coupling. For simplicity, we have assumed that the effective couplings are flavor universal and conserving for all neutrinos ν_α . For the effective couplings involving electrons, the operators $(\bar{\chi}\Gamma^i P_L \nu)(\bar{e}\Gamma_i e)$ are correlated with the operator $(\bar{\nu}\Gamma^i e)(\bar{e}\Gamma_i \chi)$ via the Fierz transformations. The latter operator can originate from the dimension-6 operators involving heavy right-handed neutrinos, if we identify χ as a heavy neutrino [115, 116].

The interactions of ν_α and χ with nucleons $N \equiv p, n$ can be constructed from the more fundamental interactions with the SM quarks, i.e. from the operators in the form of

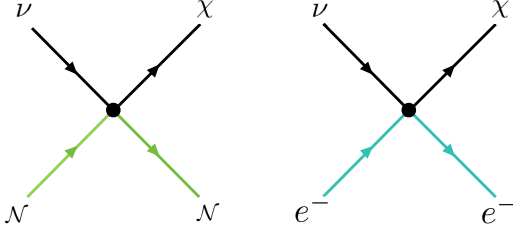


Figure 1. Feynman diagrams for the neutrino scattering off nucleus $\nu_\alpha + \mathcal{N} \rightarrow \chi + \mathcal{N}$ (left) or electron $\nu_\alpha + e \rightarrow \chi + e$ (right), induced by the effective couplings in Eq. (2.1).

$(\bar{q}\Gamma^i q)(\chi\Gamma_i P_L \nu_\alpha)$ [25, 117–120]. The SM neutrinos ν_α and dark particle χ could also couple to gluons at the 1-loop or higher order, which contributes also to the effective couplings of nucleons in Eq. (2.1) [118, 121–129]. The energy scales for the effective couplings in Eq. (2.1) are characterized by the center-of-mass energies in the experiments COHERENT [130], CONUS+ [131] and DUNE [132], which are significantly below the electroweak scale of $\mathcal{O}(100\text{ GeV})$. At such low energy scales, there might also exist the couplings of χ with charged leptons $\ell \equiv e, \mu, \tau$, i.e. in the form of $\sim (\bar{\chi}\Gamma^i \ell)(\bar{f}\Gamma_i f)$, which, however, can be very different from those involving neutrinos in Eq. (2.1). Focusing only on the couplings in Eq. (2.1), we will not consider the corresponding couplings with charged leptons in this paper.

It is possible that the nucleon couplings depend on the isospin; in other words, the cutoff scales $\Lambda_{i,p}$ and $\Lambda_{i,n}$ could have different values. In some scenarios, the couplings of protons and neutrons may even have opposite signs [133]. As a case study, we consider two distinct scenarios for the vector interaction, i.e. the isospin conserving (IC) one $\Lambda_{V,p} = \Lambda_{V,n}$ and the isospin violating (IV) one $\Lambda_{V,p} = -\Lambda_{V,n}$. For the other four Lorentz structure, i.e. the scalar, pseudo-scalar, axial-vector, and tensor interactions, we assume they are all of the IC type.

The effective couplings in Eq. (2.1) could induce the scattering of (anti)neutrinos $\nu_\alpha(\bar{\nu}_\alpha)$ with electrons e^- or nuclei \mathcal{N} in the target to produce the (anti) dark particle $\chi(\bar{\chi})$, i.e.

$$\nu_\alpha(\bar{\nu}_\alpha) + e^- \rightarrow \chi(\bar{\chi}) + e^- , \quad (2.2a)$$

$$\nu_\alpha(\bar{\nu}_\alpha) + \mathcal{N} \rightarrow \chi(\bar{\chi}) + \mathcal{N} . \quad (2.2b)$$

The corresponding representative Feynman diagrams are shown in Fig. 1. While the effective couplings are assumed to be flavor universal, the experiments considered in this work are sensitive only to the (anti)neutrino flavors of $\nu_e, \bar{\nu}_e, \nu_\mu$, and $\bar{\nu}_\mu$.

For the scattering of neutrinos with nuclei, the calculations are a bit involved, as nuclei are composite particles. The nuclear structures have to be taken into account in the corresponding differential cross sections, which are interaction dependent. Within the

nucleon level EFT description, the differential cross sections with respect to the nuclear recoil energy T_N can be written as [108, 134]:

$$\frac{d\sigma_N^S}{dT_N} = \frac{A^2 m_N}{4\pi \Lambda_{S,N}^4} F_W^2(|\mathbf{q}|^2) \left(1 + \frac{T_N}{2m_N} \right) \left(\frac{m_N T_N}{E_\nu^2} + \frac{m_\chi^2}{2E_\nu^2} \right), \quad (2.3a)$$

$$\frac{d\sigma_N^P}{dT_N} = \frac{A^2 m_N}{4\pi \Lambda_{P,N}^4} F_W^2(|\mathbf{q}|^2) \frac{T_N}{2m_N} \left(\frac{m_N T_N}{E_\nu^2} + \frac{m_\chi^2}{2E_\nu^2} \right), \quad (2.3b)$$

$$\frac{d\sigma_N^V}{dT_N} = \frac{C_V^2 m_N}{2\pi \Lambda_{V,N}^4} F_W^2(|\mathbf{q}|^2) \left[\left(1 - \frac{m_N T_N}{2E_\nu^2} - \frac{T_N}{E_\nu} + \frac{T_N^2}{2E_\nu^2} \right) - \frac{m_\chi^2}{4E_\nu^2} \left(1 + \frac{2E_\nu}{m_N} - \frac{T_N}{m_N} \right) \right], \quad (2.3c)$$

$$\begin{aligned} \frac{d\sigma_N^A}{dT_N} = & \frac{2m_N}{(2J+1)\Lambda_{A,N}^4} \left\{ \left[\left(2 + \frac{m_N T_N}{E_\nu^2} - \frac{2T_N}{E_\nu} - \frac{T_N}{m_N} + \frac{T_N^2}{2E_\nu^2} + \frac{T_N^2}{m_N E_\nu} \right) \right. \right. \\ & - \frac{m_\chi^2}{2E_\nu^2} \left(1 + \frac{3E_\nu}{m_N} + \frac{m_\chi^2}{m_N T_N} - \frac{T_N}{2m_N} \right) \left. \right] \tilde{S}^T(|\mathbf{q}|^2) \\ & + 2 \left[\frac{T_N}{E_\nu} \left(\frac{E_\nu}{m_N} - \frac{T_N}{2E_\nu} - \frac{T_N}{m_N} \right) + \frac{m_\chi^2}{2E_\nu^2} \left(2 + \frac{3E_\nu}{m_N} + \frac{m_\chi^2}{m_N T_N} - \frac{T_N}{2m_N} \right) \right] \tilde{S}^L(|\mathbf{q}|^2) \left. \right\}, \end{aligned} \quad (2.3d)$$

$$\begin{aligned} \frac{d\sigma_N^T}{dT_N} = & \frac{m_N}{(2J+1)\Lambda_{T,N}^4} \left\{ \left[\left(2 - \frac{m_N T_N}{E_\nu^2} - \frac{2T_N}{E_\nu} + \frac{T_N}{m_N} - \frac{T_N^2}{m_N E_\nu} - \frac{T_N^2}{E_\nu^2} \right) \right. \right. \\ & + \frac{m_\chi^2}{2E_\nu^2} \left(1 + \frac{3E_\nu}{m_N} - \frac{T_N}{m_N} + \frac{m_\chi^2}{m_N T_N} \right) \left. \right] \tilde{S}^T(|\mathbf{q}|^2) \\ & + \left[\left(1 - \frac{T_N}{E_\nu} - \frac{T_N}{2m_N} + \frac{T_N^2}{2E_\nu^2} + \frac{T_N^2}{2m_N E_\nu} \right) \right. \\ & - \frac{m_\chi^2}{2E_\nu^2} \left(1 + \frac{3E_\nu}{2m_N} - \frac{T_N}{2m_N} + \frac{m_\chi^2}{2m_N T_N} \right) \left. \right] \tilde{S}^L(|\mathbf{q}|^2) \left. \right\}, \end{aligned} \quad (2.3e)$$

where m_N is the nucleus mass, J is the nuclear spin, A is the mass number of nucleus, and C_V is the coefficient for the vector coupling. The function $F_W(|\mathbf{q}|^2)$ is the weak nuclear form factor accounting for the finite-size effects while $\tilde{S}^T(|\mathbf{q}|^2)$ and $\tilde{S}^L(|\mathbf{q}|^2)$ denote the transverse and longitudinal nuclear spin structure functions, respectively, which encode the spin-dependent nuclear response after combining proton and neutron couplings at the nucleon level. More details of the form factors and spin structure functions are collected in Appendix A.

It is transparent from Eq. (2.3a) and Eq. (2.3b) that, for scalar and pseudoscalar interactions, the scattering amplitudes add coherently over nucleons inside the target nucleus, leading to an overall enhancement proportional to A^2 , in close analogy with the CE ν NS (Coherent Elastic Neutrino-Nucleus Scattering) processes. The corresponding (differential) cross sections are therefore enhanced by the atomic number A^2 of target nuclei. At the nucleon level, the coherent effective charge C_V depends on the relative sign between the proton and neutron couplings. So, for the vectorial couplings, the coefficient in Eq. (2.3c)

is

$$C_V = \begin{cases} A, & \text{isospin conserving,} \\ Z - N, & \text{isospin violating,} \end{cases} \quad (2.4)$$

with Z and N being the proton and neutron numbers inside the nucleus, respectively. For the IV case with $\Lambda_{V,p} = -\Lambda_{V,n}$, the proton and neutron couplings cancel partially with each other in the coherent sum, which leads to a significant suppression of the cross section with respect to the IC case. As a result, the corresponding sensitivities of the IV cases depend critically on the neutron excess ($N - Z$) of the target material. For the axial-vector and tensor interactions, as shown in Eq. (2.3d) and Eq. (2.3e), the scattering is governed by the spin structures of the nucleus rather than by the total nucleon number.

For the electron target, it is straightforward to calculate the differential cross sections, with respect to the recoil energy T_e of electron [9, 89]:

$$\frac{d\sigma_e^S}{dT_e} = \frac{m_e}{4\pi\Lambda_{S,e}^4} \left(1 + \frac{T_e}{2m_e} \right) \left(\frac{m_e T_e}{E_\nu^2} + \frac{m_\chi^2}{2E_\nu^2} \right), \quad (2.5a)$$

$$\frac{d\sigma_e^P}{dT_e} = \frac{m_e}{4\pi\Lambda_{P,e}^4} \frac{T_e}{2m_e} \left(\frac{m_e T_e}{E_\nu^2} + \frac{m_\chi^2}{2E_\nu^2} \right), \quad (2.5b)$$

$$\frac{d\sigma_e^V}{dT_e} = \frac{m_e}{2\pi\Lambda_{V,e}^4} \left[\left(1 - \frac{m_e T_e}{2E_\nu^2} - \frac{T_e}{E_\nu} + \frac{T_e^2}{2E_\nu^2} \right) - \frac{m_\chi^2}{4E_\nu^2} \left(1 + \frac{2E_\nu}{m_e} - \frac{T_e}{m_e} \right) \right], \quad (2.5c)$$

$$\frac{d\sigma_e^A}{dT_e} = \frac{m_e}{2\pi\Lambda_{A,e}^4} \left[\left(1 + \frac{m_e T_e}{2E_\nu^2} - \frac{T_e}{E_\nu} + \frac{T_e^2}{2E_\nu^2} \right) + \frac{m_\chi^2}{4E_\nu^2} \left(1 - \frac{2E_\nu}{m_e} + \frac{T_e}{m_e} \right) \right], \quad (2.5d)$$

$$\frac{d\sigma_e^T}{dT_e} = \frac{4m_e}{\pi\Lambda_{T,e}^4} \left[\left(1 - \frac{m_e T_e}{4E_\nu^2} - \frac{T_e}{E_\nu} + \frac{T_e^2}{4E_\nu^2} \right) - \frac{m_\chi^2}{4E_\nu^2} \left(\frac{1}{2} + \frac{2E_\nu}{m_e} - \frac{T_e}{2m_e} \right) \right]. \quad (2.5e)$$

where m_e is the electron mass, E_ν is the incident neutrino energy, and m_χ is the dark particle mass.

2.2 Dark particle decay

It is apparent in Eq. (2.1) that the stability of dark particle χ is not guaranteed, which, on contrary, leads inevitably to the decay of χ . For the mass range of $m_\chi > 2m_e$, the interactions with electrons lead to the decay of χ into a neutrino and an electron-positron pair, i.e.

$$\chi \rightarrow \nu_\alpha + e^+ + e^- . \quad (2.6)$$

The corresponding partial width [18] is

$$\Gamma(\chi \rightarrow \nu_\alpha e^+ e^-) \simeq \frac{m_\chi^5}{192\pi^3\Lambda_{i,e}^4} \left(1 - \frac{4m_e^2}{m_\chi^2} \right)^{3/2}, \quad (2.7)$$

which is heavily suppressed by the cutoff scale $\Lambda_{i,e}$. The corresponding proper decay length τ_χ of the dark particle is much longer than the laboratory distances we are interested in

throughout this paper. For instance,

$$\tau_\chi \simeq 5 \times 10^8 \text{ cm} \left(\frac{m_\chi}{30 \text{ MeV}} \right)^{-5} \left(\frac{\Lambda_{i,e}}{1 \text{ TeV}} \right)^4. \quad (2.8)$$

At the one-loop order, the visible decays of χ into a neutrino ν_α plus photon(s) and the invisible decay of χ into three neutrinos are possible [10, 11]:

$$\chi \rightarrow \nu_\alpha \gamma, \quad \chi \rightarrow \nu_\alpha \gamma \gamma, \quad \chi \rightarrow \nu_\alpha \gamma \gamma \gamma, \quad \chi \rightarrow \nu_\alpha \nu \bar{\nu}, \quad (2.9)$$

depending on the Lorentz structure. These decays are also kinematically allowed for a light χ with mass below the MeV scale. The two-body decay $\chi \rightarrow \nu_\alpha \gamma$ is only allowed for the tensor coupling, while it is forbidden for other couplings by the charge conjugation symmetry of quantum electrodynamics. In the tensor coupling case, the partial width is [11]

$$\Gamma^T(\chi \rightarrow \nu_\alpha \gamma) = \frac{\alpha m_e^2 m_\chi^3}{16\pi^4 \Lambda_{T,e}^4} \log^2 \left(\frac{\Lambda_{T,e}^2}{m_e^2} \right), \quad (2.10)$$

with α being the fine structure constant. The corresponding lifetime is also highly suppressed by the cutoff scale $\Lambda_{T,e}$ as well as the loop factor,

$$\tau_\chi^{T,e} \simeq 6 \times 10^{11} \text{ cm} \left(\frac{m_\chi}{30 \text{ MeV}} \right)^{-3} \left(\frac{\Lambda_{T,e}}{1 \text{ TeV}} \right)^4 \left(\frac{\log^2(\Lambda_{T,e}^2/m_e^2)}{1000} \right). \quad (2.11)$$

As detailed in Ref. [11], the lifetimes due to the three- and four-body decays at the 1-loop order in Eq. (2.9) are much longer than the two-body decay $\chi \rightarrow \nu_\alpha \gamma$.

Let us now move to the couplings of χ and neutrinos with nucleons. The dark particle χ in this paper has a mass below the GeV scale, and the decay channel $\chi \rightarrow \nu_\alpha NN$ is kinematically forbidden. All the 1-loop decays above can also be induced, with the electron in the loops replaced by a proton. Substituting the electron mass m_e in Eq. (2.10) by the nucleon mass m_N , the resultant lifetime is

$$\tau_\chi^{T,p} \simeq 6 \times 10^5 \text{ cm} \left(\frac{m_\chi}{30 \text{ MeV}} \right)^{-3} \left(\frac{\Lambda_{T,N}}{1 \text{ TeV}} \right)^4 \left(\frac{\log^2(\Lambda_{T,N}^2/m_N^2)}{200} \right), \quad (2.12)$$

which is long enough for χ to decay outside the detectors for the parameter space of interest. Again, it is expected that with the couplings to nucleons, the partial widths of the three- and four-body decays in Eq. (2.9) are suppressed by the phase space, with respect to the two-body decay. In short, for the purpose of this paper, the dark particle χ leaves the detectors without leaving any signal for the parameter space we are interested in, for both the couplings to electron and nucleons.

2.3 Kinematic analysis

The inelastic scattering process in Eq. (2.2a) and Eq. (2.2b) features a kinematic threshold governed by the dark particle mass m_χ and the target mass m_T (m_e for electrons or m_N for nuclei). For a given recoil kinetic energy T_r of the target particle, the minimum incident

neutrino energy required to produce χ is obtained from the four-momentum conservation and the mass on-shell conditions [89]:

$$E_\nu^{\min}(m_\chi, T_r) = \frac{1}{2} \left(T_r + \sqrt{2m_T T_r + T_r^2} \right) \left(1 + \frac{m_\chi^2}{2m_T T_r} \right). \quad (2.13)$$

Here $\sqrt{2m_T T_r + T_r^2} = |\mathbf{p}'|$ is the three-momentum of the recoiling target particle, which implies that the required energy depends on both the dark particle mass m_χ and the recoil energy T_r . This expression reduces to the well known elastic scattering limit when $m_\chi = 0$. Conversely, for a fixed neutrino energy E_ν , the kinematically allowed recoil energy T_r is bounded. Solving the energy and momentum conservation equations for T_r gives the maximum and minimum recoil energies:

$$T_{\max}(m_\chi, E_\nu) = \frac{2m_T E_\nu^2 - m_\chi^2(E_\nu + m_T) + E_\nu \sqrt{\Delta}}{2m_T(2E_\nu + m_T)}, \quad (2.14a)$$

$$T_{\min}(m_\chi, E_\nu) = \frac{2m_T E_\nu^2 - m_\chi^2(E_\nu + m_T) - E_\nu \sqrt{\Delta}}{2m_T(2E_\nu + m_T)}, \quad (2.14b)$$

where

$$\Delta \equiv 4m_T^2 E_\nu^2 - 4m_T m_\chi^2 (E_\nu + m_T) + m_\chi^4. \quad (2.15)$$

These relations apply to the scatterings involving both electrons and nuclei.

The kinematic upper bound on the dark particle mass m_χ is determined by energy momentum conservation and the maximal available neutrino energy. In the limit of vanishing recoil energy $T_r \rightarrow 0$, the kinematic upper bound is [89]

$$m_\chi \lesssim \sqrt{m_T(m_T + 2E_\nu)} - m_T, \quad (2.16)$$

This bound corresponds to the point of $T_{\min} = T_{\max}$, and therefore represents the maximal dark particle mass that can be produced. This kinematic constraint allows to estimate the maximal dark particle mass that can be probed at different neutrino experiments. At the DUNE experiment, the neutrino energy can reach $\mathcal{O}(10 \text{ GeV})$ [132], which implies sensitivity to dark particle masses up to $\mathcal{O}(100) \text{ MeV}$. For COHERENT and CONUS+ experiments, the nuclear target masses are much larger than the neutrino energies. In this regime, Eq. (2.16) can be simplified to $m_\chi \lesssim E_\nu^{\max}$, indicating that almost the entire neutrino energy carried by the incoming neutrino is nearly all converted to be the dark particle mass in the final state. For COHERENT at the SNS, the neutrino energies are about 50 MeV [130]. In CONUS+, reactor antineutrinos exhibit lower energies below $\sim 12 \text{ MeV}$ [131].

The typical momentum transfer in the scattering process, $|\mathbf{q}| \simeq \sqrt{2m_T T_r}$ plays an important role in assessing the validity of the EFT description. In the framework of EFT the cutoff scale Λ is required to satisfy $\Lambda \gg |\mathbf{q}|$ to ensure the point-like interaction approximation. It turns out that the experiments COHERENT, CONUS+ and DUNE ND probe distinct momentum transfer regimes due to their different targets and recoil energy sensitivities:

- For the spallation source CE ν NS experiment COHERENT, the target is CsI, with nuclear masses $m_{\text{Cs}} \simeq 124 \text{ GeV}$ and $m_{\text{I}} \simeq 118 \text{ GeV}$, and typical nuclear recoil energies $T_{\mathcal{N}} \sim \text{few tens of keV}$. This implies a characteristic momentum transfer $|\mathbf{q}| \simeq \sqrt{2m_{\mathcal{N}}T_{\mathcal{N}}} \sim \mathcal{O}(10-100) \text{ MeV}$ [130].
- For the reactor neutrino experiment CONUS+, with a germanium target $m_{\text{Ge}} \simeq 66 \text{ GeV}$ and nuclear recoil energies $T_{\mathcal{N}} \sim \mathcal{O}(0.1-1) \text{ keV}$, the characteristic momentum transfer is $|\mathbf{q}| \sim \mathcal{O}(1-10) \text{ MeV}$ [131].
- In the DUNE experiment, the accelerator neutrino energies are much higher, and the electron recoil energy T_e ranges from $\sim 30 \text{ MeV}$ to several GeV [132]. However, for the momentum transfer is given by $|\mathbf{q}| \simeq \sqrt{2m_eT_e}$. As a result, even for electron recoil energies at the GeV scale, the momentum transfer remains well below the GeV scale, typically $\mathcal{O}(10-50) \text{ MeV}$.

As we will see in Fig. 5 and Fig. 6, the COHERENT and CONUS+ limits on the cutoff scales and the prospects at DUNE ND are all well above the corresponding characteristic transferred momenta, unless the dark particle mass is close to the kinematic threshold, where larger recoil energies (and hence larger $|\mathbf{q}|$) are required. This indicates that the EFT description in this paper is valid.

3 Analysis details

In this section, we provide all the analysis details for estimating the limits on the cutoff scales from the current COHERENT data in Sec. 3.1 and the CONUS+ data in Sec. 3.2. The analysis details for the DUNE ND sensitivities are given in Sec. 3.3.

3.1 COHERENT

We analyze the CsI detector dataset released by the COHERENT collaboration in 2021 [135]. The CsI detector has a fiducial mass $m_{\text{det}} = 14.57 \text{ kg}$ and is located at a distance $L = 19.3 \text{ m}$ from the Spallation Neutron Source (SNS) [135, 136]. Neutrinos are produced via pion decay at rest, giving rise to a pulsed flux consisting of a prompt mono-energetic ν_{μ} component from $\pi^+ \rightarrow \mu^+ \nu_{\mu}$, followed by delayed ν_e and $\bar{\nu}_{\mu}$ components from muon decay. The neutrino energy spectra and flavor dependent timing distributions are taken from the official COHERENT CsI-2021 data release [135, 137]. A similar study can be found in Ref. [8], which is, however based on the early COHERENT data [136].

The experimental observables are the reconstructed number of photoelectrons n_{PE} and the reconstructed arrival time t_{rec} . Following the COHERENT collaboration, we perform a binned two-dimensional analysis in the $(n_{\text{PE}}, t_{\text{rec}})$ plane [80, 108, 135]. For a given neutrino flavor ν_{α} and nuclear target $\mathcal{N} = \text{Cs}$ or I , the differential event rate with respect to the nuclear recoil energy $T_{\mathcal{N}}$ is

$$\frac{dN_{\nu_{\alpha}\mathcal{N}}}{dT_{\mathcal{N}}} = N_{\text{target}} \int_{E_{\nu}^{\text{min}}(T_{\mathcal{N}})}^{E_{\nu}^{\text{max}}} dE_{\nu} \frac{d\Phi_{\nu_{\alpha}}}{dE_{\nu}}(E_{\nu}) \frac{d\sigma_{\nu_{\alpha}\mathcal{N}}}{dT_{\mathcal{N}}}(E_{\nu}, T_{\mathcal{N}}), \quad (3.1)$$

where $N_{\text{target}} \equiv N_A m_{\text{det}} / M_{\mathcal{N}}$ is the number of target nuclei. The contributions from the Cs and I nuclei are computed separately and combined according to their corresponding target numbers in the CsI crystal.

The nuclear recoil energy is converted into an electron-equivalent energy E_{ee} through the energy dependent quenching factor $Q(T_{\mathcal{N}})$ via

$$E_{ee} = Q(T_{\mathcal{N}}) T_{\mathcal{N}}, \quad (3.2)$$

where $Q(T_{\mathcal{N}})$ is taken from the COHERENT CsI-2021 release and parameterized as a fourth-order polynomial using the neutron calibration data [135]. The electron-equivalent energy is subsequently converted into the mean number of photoelectrons using a fixed light yield,

$$\bar{n}_{\text{PE}} = Y E_{ee}, \quad \text{with} \quad Y = 13.35 \text{ PE/keV}_{ee}. \quad (3.3)$$

The detector effects, including photoelectron statistics, energy resolution, and the n_{PE} -dependent detection efficiency $\epsilon_E(n_{\text{PE}})$, are implemented through the response kernel $\mathcal{R}(n_{\text{PE}} | T_{\mathcal{N}})$ following the official COHERENT CsI-2021 prescription [80, 108, 135]. The SNS neutrino flux exhibits a pronounced time structure. For each neutrino flavor ν_{α} , we adopt the arrival time probability density $P_T^{\nu_{\alpha}}(t)$ by the COHERENT collaboration, and the reconstructed time t_{rec} is implemented together with the time dependent efficiency $\epsilon_T(t_{\text{rec}})$ following the CsI-2021 prescription. The explicit functional forms and numerical parameters entering $\mathcal{R}(n_{\text{PE}} | T_{\mathcal{N}})$, ϵ_E , $P_T^{\nu_{\alpha}}$, and ϵ_T are taken from the supplemental material of Ref. [135].

The expected number of CE ν NS events in the (i, j) -th bin of $(n_{\text{PE}}, t_{\text{rec}})$ is given by

$$\begin{aligned} \mathcal{N}_{ij}^{\text{CE}\nu\text{NS}} &= \sum_{\nu_{\alpha}} \sum_{\mathcal{N}=\text{Cs,I}} \int dT_{\mathcal{N}} \frac{dN_{\nu_{\alpha}\mathcal{N}}}{dT_{\mathcal{N}}} \int dn_{\text{PE}} \mathcal{I}_i(n_{\text{PE}}) \epsilon_E(n_{\text{PE}}) \mathcal{R}(n_{\text{PE}} | T_{\mathcal{N}}) \\ &\quad \times \int dt_{\text{rec}} \mathcal{I}_j(t_{\text{rec}}) \epsilon_T(t_{\text{rec}}) P_T^{\nu_{\alpha}}(t_{\text{rec}}), \end{aligned} \quad (3.4)$$

where \mathcal{I}_i and \mathcal{I}_j denote the indicator functions for the i -th n_{PE} bin and the j -th time bin, respectively. In the CsI-2021 analysis, the reconstructed photoelectron axis is divided into 9 bins and the reconstructed time axis is divided into 11 bins, yielding a total of 9×11 bins. The bin boundaries follow exactly those adopted in the official COHERENT CsI-2021 release [135]. All expected event numbers entering the likelihood analysis are evaluated in the corresponding $(n_{\text{PE}}, t_{\text{rec}})$ bins.

The experimental background components, including the beam-related neutrons (BRN), neutrino-induced neutrons (NIN), and steady-state background (SSB), are taken directly from the templates provided by the COHERENT collaboration [135]. Although the elastic neutrino-electron scattering (E ν ES) may in principle contribute due to the lack of recoil discrimination in CsI, we do not model E ν ES as an independent component, since its impact is subdominant for the CsI-2021 analysis window and does not affect too much the the limits on the NP parameters. This effect can be effectively absorbed into the background normalization and systematic uncertainties [80, 108].

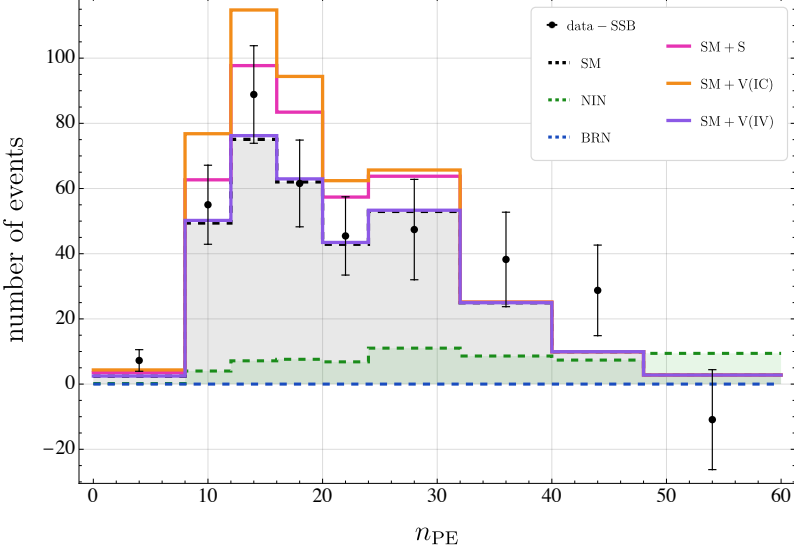


Figure 2. Event numbers at the COHERENT experiment (CsI-2021 dataset) for the SM CE ν NS process (black dashed), the NIN (green dashed) and BRN (blue dashed) backgrounds as well as the NP scenarios with the scalar (pink solid), IC (orange solid) or IV (purple solid) vector coupling, as functions of n_{PE} . The data with error bars are for the residual events after subtracting the SSB background. The backgrounds are labeled by the dashed lines with shaded regions, while the NP cases are depicted as the solid lines. We have set the parameters $m_\chi = 10$ MeV and $\Lambda = 500$ GeV.

The event distributions for the SM CE ν NS process and the BRN and NIN backgrounds for different values of n_{PE} are presented as the dashed lines with shaded regions in Fig. 2, where we have integrated over the reconstructed time. For illustration purpose, the expected events with the NP scenarios of the scalar, IC vector and IV vector couplings are depicted as the solid purple, green and blue lines, respectively. We have taken $m_\chi = 10$ MeV and $\Lambda_{i,N} = 500$ GeV for all these scenarios. The data with errors are for the events after subtracting the SSB background. It is clear in Fig. 2 that the NP contributions could significantly affect the neutrino-nucleus scattering at the COHERENT experiment and are thus constrained by the experimental data, depending on the interaction type and cutoff scale.

Based on the full two-dimensional $(n_{\text{PE}}, t_{\text{rec}})$ distributions described above, the total theoretical prediction within each (i, j) bin can be written as

$$\mathcal{N}_{ij}^{\text{th}} = (1 + \alpha_0 + \alpha_5) (\mathcal{N}_{ij}^{\text{CE}\nu\text{NS}} + \mathcal{N}_{ij}^{\text{NP}}) + (1 + \alpha_1) \mathcal{N}_{ij}^{\text{BRN}} + (1 + \alpha_2) \mathcal{N}_{ij}^{\text{NIN}} + (1 + \alpha_3) \mathcal{N}_{ij}^{\text{SSB}}, \quad (3.5)$$

where $\mathcal{N}_{ij}^{\text{CE}\nu\text{NS}}$ stands for the SM CE ν NS contribution [134, 138], and $\mathcal{N}_{ij}^{\text{NP}}$ is for the NP contribution due to the absorption operators in Eq. (2.1). The nuisance parameters α_k account for the dominant systematic uncertainties: $\sigma_0 = 11\%$ for the overall flux and efficiency normalization, $\sigma_1 = 25\%$, $\sigma_2 = 35\%$, and $\sigma_3 = 2.1\%$ for the BRN, NIN, and SSB normalizations, respectively, while $\sigma_5 = 3.8\%$ is for the quenching factor uncertainty. Addi-

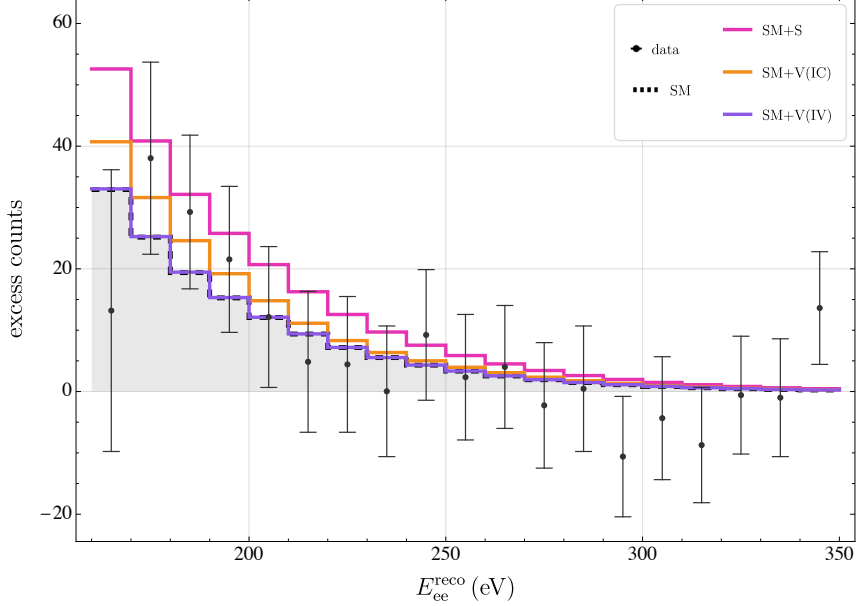


Figure 3. Binned CONUS+ excess spectra as functions of the reconstructed energy E_{ee}^{reco} , for the SM CE ν NS process (dashed black line with shaded region), and the NP scenarios with the scalar, IC or IV vector coupling (solid colored lines), as functions of E_{ee}^{reco} . The data with error bars are the measured spectrum. We have set the parameters $m_\chi = 5$ MeV and $\Lambda = 500$ GeV.

tional nuisance parameters associated with the nuclear form factor and timing uncertainties are treated following the COHERENT CsI-2021 prescription [108, 135].

To set limits on the NP contributions, we construct a binned Poisson likelihood in the two-dimensional (n_{PE}, t_{rec}) space [108, 135]:

$$\chi^2 = 2 \sum_{i,j} \left[\mathcal{N}_{ij}^{\text{th}} - \mathcal{N}_{ij}^{\text{obs}} + \mathcal{N}_{ij}^{\text{obs}} \log \left(\frac{\mathcal{N}_{ij}^{\text{obs}}}{\mathcal{N}_{ij}^{\text{th}}} \right) \right] + \sum_k \left(\frac{\alpha_k}{\sigma_k} \right)^2, \quad (3.6)$$

where $\mathcal{N}_{ij}^{\text{obs}}$ denotes the observed number of events. All the nuisance parameters are profiled to derive constraints on the NP parameters.

3.2 CONUS+

The CONUS+ experiment operates at a baseline of $L \simeq 20.7$ m from the Leibstadt nuclear power plant in Switzerland, which provides a high reactor $\bar{\nu}_e$ flux at the detector location of $\phi_{\bar{\nu}_e} \simeq 1.5 \times 10^{13} \text{ cm}^{-2} \text{ sec}^{-1}$. The detector array consists of three high-purity germanium (HPGe) detectors (C2, C3, C5) with fiducial masses 0.95 kg, 0.94 kg and 0.94 kg, respectively, amounting to a total active mass of 2.83 ± 0.02 kg. The corresponding analysis thresholds are $T_e^{\text{th}} = 160 \text{ eV}_{ee}$ (C3), 170 eV_{ee} (C5) and 180 eV_{ee} (C2) [139, 140]. After data quality selections, the exposure amounts to $327 \text{ kg} \cdot \text{day}$ (reactor on) and $60 \text{ kg} \cdot \text{day}$ (reactor off) [139]. The low energy thresholds and high reactor neutrino flux make CONUS+ particularly sensitive to low-energy neutrino interactions, including the SM CE ν NS process and possible NP contributions in the nuclear recoil channel.

In this work, we follow the one-dimensional spectral analysis strategy [141] based on the reconstructed ionization energy spectrum. In the estimates of the CONUS+ limits of the NP contributions, we adopt a CE ν NS-only treatment, which is consistent with the fact that the NP effects at the CONUS+ experiments are dominated by the nuclear channel. The CE ν NS+E ν ES choice can lead to small differences in the light mass regime in some NP cases [141].

The predicted differential rate in the reconstructed ionization energy E_e^{reco} is obtained by convolving the reactor $\bar{\nu}_e$ flux with the differential cross section and the detector response,

$$\frac{d\mathcal{R}}{dE_{\text{ee}}^{\text{reco}}} = \mathcal{E} \int dT_{\mathcal{N}} \mathcal{G}(E_{\text{ee}}^{\text{reco}}, E_{\text{er}}) \int dE_{\nu} \frac{d\phi}{dE_{\nu}} \frac{d\sigma_{\bar{\nu}_e \mathcal{N}}}{dT_{\mathcal{N}}}, \quad (3.7)$$

where \mathcal{E} denotes the exposure, and \mathcal{G} is the energy resolution kernel [140, 141], E_{er} is the true electron-equivalent recoil energy, and the integration bounds of the nuclear recoil energy are determined by the detector threshold through the quenching relation, and by the kinematic maximum recoil energy for a given neutrino energy. The energy resolution function is modeled as a Gaussian distribution,

$$\mathcal{G}(E_{\text{ee}}^{\text{reco}}, E_{\text{er}}) \equiv \frac{1}{\sqrt{2\pi}\sigma_{\text{res}}} \exp \left[-\frac{(E_{\text{ee}}^{\text{reco}} - E_{\text{er}})^2}{2\sigma_{\text{res}}^2} \right], \quad (3.8)$$

with the resolution width given by [140, 142]:

$$\sigma_{\text{res}} \equiv \sqrt{\sigma_0^2 + \mathcal{F}_{\text{fano}}\eta E_{\text{er}}}. \quad (3.9)$$

Here $\sigma_0 = 20.38 \text{ eV}_{\text{ee}}$ (derived from a full width at half maximum of 48 eV_{ee}), $\mathcal{F}_{\text{fano}} = 0.1096$ is the Fano factor for germanium [139], and $\eta = 2.96 \text{ eV}_{\text{ee}}$ is the average energy required to create an electron-hole pair. The true nuclear recoil energy $T_{\mathcal{N}}$ is related to the electron-equivalent energy E_{er} via the quenching factor Q_{QF} :

$$E_{\text{er}} = Q_{\text{QF}}(T_{\mathcal{N}})T_{\mathcal{N}} = \frac{kg(\epsilon)}{1+kg(\epsilon)}T_{\mathcal{N}}, \quad (3.10)$$

where $\epsilon = 11.5Z^{-7/3}T_{\mathcal{N}}$, $g(\epsilon) = 3\epsilon^{0.15} + 0.7\epsilon^{0.6} + \epsilon$, and $k = 0.162 \pm 0.004$ is the Lindhard parameter [143]. Using this relation, the differential cross section with respect to E_{er} can be straightforwardly obtained from the nuclear recoil cross section in Eq. (2.3). The reactor antineutrino spectrum $d\phi/dE_{\nu}$ is constructed using the spectral function from Ref. [144] for $E_{\nu} < 2 \text{ MeV}$ and from Ref. [145] for higher energies.

The predicted number of events in each reconstructed energy bin is:

$$\mathcal{R}_i^{\text{th}} = \int_i \frac{d\mathcal{R}}{dE_{\text{ee}}^{\text{reco}}} dE_{\text{ee}}^{\text{reco}}, \quad (3.11)$$

which includes both the SM CE ν NS and NP contributions, i.e.

$$\mathcal{R}_i^{\text{th}} = \mathcal{R}_i^{\text{CE}\nu\text{NS}} + \mathcal{R}_i^{\text{NP}}. \quad (3.12)$$

For illustration purpose, the spectra for the pure SM process and those for the scalar, IC vector and IV vector NP cases are shown in Fig. 3 as the dotted and solid purple, green and blue lines, respectively, as functions of the reconstructed energy E_{ee}^{reco} . For the NP scenarios we have taken the benchmark values of $m_\chi = 5 \text{ MeV}$ and $\Lambda_{i,N} = 500 \text{ GeV}$. As in Fig. 2, the spectra might be disturbed by the NP $\bar{\nu}_e \mathcal{N} \rightarrow \bar{\chi} \mathcal{N}$ scattering.

The statistical analysis is performed by using the χ^2 function [140, 142]:

$$\chi^2 = \sum_i \frac{[\mathcal{R}_i^{\text{exp}} - (1 + \alpha)\mathcal{R}_i^{\text{th}}]^2}{\sigma_i^2} + \left(\frac{\alpha}{\sigma_\alpha}\right)^2, \quad (3.13)$$

where α is a nuisance parameter accounting for the combined systematic uncertainty with $\sigma_\alpha = 16.9\%$. This uncertainty incorporates contributions from the reactor antineutrino flux (4.6%), quenching factor (7.3%), energy threshold (14.1%), active detector mass (1.1%), trigger efficiency (0.7%), and nuclear form factor (3.2%) [140, 142]. The CONUS+ collaboration reports 395 ± 106 CE ν NS events [140], consistent with the SM prediction of 347 ± 59 events, which allows us to derive constraints on the NP parameter space.

3.3 DUNE Near Detector

DUNE is a next-generation long baseline neutrino oscillation experiment. Its ND complex, located at Fermilab, will be exposed to the high-intensity neutrino beam produced by the Long-Baseline Neutrino Facility (LBNF) [132]. The ND is equipped with a Liquid Argon Time Projection Chamber (LArTPC), with a fiducial mass about 67 tons and excellent particle identification capabilities. The DUNE ND design supports the Precision Reaction Independent Spectrum Measurement (PRISM) program, where the ND liquid Argon system can be moved transversely with respect to the beam to sample off-axis fluxes (up to 30 m from the beam axis) [146]. For simplicity we consider conservatively only the on-axis (0 m) configuration, which receives the highest neutrino fluxes and dominates the expected event rate. This simplification provides rather conservative sensitivities of DUNE ND, as inclusion of the off-axis data would definitely suppress the spectral uncertainties and improve the overall statistical power.

The DUNE neutrino beam is composed of $\nu_e, \bar{\nu}_e, \nu_\mu, \bar{\nu}_\mu$ with GeV energies under both the neutrino and anti-neutrino modes [132]. The corresponding on-axis neutrino fluxes can be found in Refs. [147–149]. The total number of protons on target (POT) per year is expected to be $N_{\text{POT}} = 1.1 \times 10^{21}$ [146, 150]. As discussed in Ref. [151], the electron detection threshold T_e^{min} can be as low as 30 MeV [152]. So in the analysis we set the range of $T_e \geq T_e^{\text{min}}$.

At the DUNE ND, the signal process produces a final-state electron that is experimentally indistinguishable from the elastic $\nu(\bar{\nu})-e^-$ scattering. Therefore, the SM $\nu(\bar{\nu})-e^-$ scattering constitutes the dominant irreducible background. The reducible backgrounds arise from the charged-current quasi-elastic (CCQE) neutrino scattering and mis-identified π^0 events [153, 154], whose contributions can be effectively suppressed by the cut on the variable $E_e \theta_e^2$, where $E_e \equiv m_e + T_e$ and θ_e are the electron total energy and scattering

angle, respectively. The kinematic relation is given by

$$1 - \cos \theta_e = \frac{m_e}{E_e} (1 - y), \quad (3.14)$$

where the inelasticity $y \equiv T_e/E_\nu$ is for the SM $\nu(\bar{\nu})$ - e^- scattering. For the inelastic scattering processes, the inelasticity becomes [89]

$$y \equiv \frac{T_e}{E_\nu} \left[1 + \frac{m_\chi^2}{2m_e T_e} \right]. \quad (3.15)$$

The energy resolution of the LArTPC detector is estimated to be $\sigma_{E_e}/E_e \simeq 10\%/\sqrt{E_e/\text{GeV}}$, which has a negligible impact on our analysis [89, 149, 155]. The angular resolution is taken to be $\sigma_\theta = 1^\circ$ [146, 155].

The number of events at the DUNE ND as a function of $E_e \theta_e^2$ can be calculated as [89]:

$$\frac{d\mathcal{N}}{d(E_e \theta_e^2)} = t_{\text{run}} N_e N_{\text{POT}} \sum_{\alpha} \int_{E_\nu^{\text{min}}}^{E_\nu^{\text{max}}} dE_\nu \frac{d\Phi_{\nu_\alpha}(E_\nu)}{dE_\nu} \frac{d\sigma_{\nu_\alpha}}{d(E_e \theta_e^2)}, \quad (3.16)$$

where the differential cross section is

$$\frac{d\sigma_{\nu_\alpha}}{d(E_e \theta_e^2)} = \frac{E_\nu}{2m_e} \frac{d\sigma_{\nu_\alpha}}{dT_e} \Big|_{T_e}. \quad (3.17)$$

Here we have set $t_{\text{run}} = 7$ years (3.5 years in ν mode plus 3.5 years in $\bar{\nu}$ mode), N_e is the number of electron targets in the LArTPC detector, $d\Phi_{\nu_\alpha}/dE_\nu$ is the (anti)neutrino flux for the different neutrino flavors $\nu_\alpha = \{\nu_e, \nu_\mu, \bar{\nu}_e, \bar{\nu}_\mu\}$, and T_e^{max} is determined by kinematics. The differential distributions for the SM $\nu(\bar{\nu})$ - e^- elastic scattering, the CCQE and mis-identified π^0 backgrounds, and the NP signal contributions are shown in Fig. 4 as functions of $x \equiv E_e \theta_e^2$. The left and right panels are for the neutrino and antineutrino modes, respectively. For all the NP scenarios with the five Lorentz structures, we have set the benchmark values of $m_\chi = 10$ MeV and $\Lambda_{i,e} = 650$ GeV. All spectra are normalized to one year of exposure and are grouped into 12 bins in the range of $x \in [0, 3] \text{ MeV} \cdot \text{rad}^2$. The SM $\nu(\bar{\nu})$ - e^- elastic scattering cross sections used in our analysis follow the standard electroweak expressions, which can be found in e.g. Ref. [156].

The DUNE ND sensitivities are estimated by performing a χ^2 analysis using 12 bins in $E_e \theta_e^2$ [89, 154]. The χ^2 function is defined as:

$$\chi^2 = 2 \sum_{i=1}^{12} \left[\mathcal{N}_i^{\text{th}} - \mathcal{N}_i^{\text{exp}} + \mathcal{N}_i^{\text{exp}} \log \left(\frac{\mathcal{N}_i^{\text{exp}}}{\mathcal{N}_i^{\text{th}}} \right) \right] + \left(\frac{\alpha_1}{\sigma_{\alpha_1}} \right)^2 + \left(\frac{\alpha_2}{\sigma_{\alpha_2}} \right)^2, \quad (3.18)$$

where i is the index for the 12 bins, and

$$\mathcal{N}^{\text{th}} \equiv (1 + \alpha_1) \mathcal{N}_{\text{SM}} + (1 + \alpha_2) \mathcal{N}_{\text{bkg}} + \mathcal{N}_{\text{NP}}, \quad (3.19a)$$

$$\mathcal{N}^{\text{exp}} \equiv \mathcal{N}_{\text{SM}} + \mathcal{N}_{\text{bkg}}, \quad (3.19b)$$

with $\mathcal{N}_{\text{SM, bkg, NP}}$ the numbers of events for the SM $\nu(\bar{\nu})$ - e^- scattering, the CCQE and π^0 mis-identification backgrounds, and the NP contributions, respectively. The nuisance

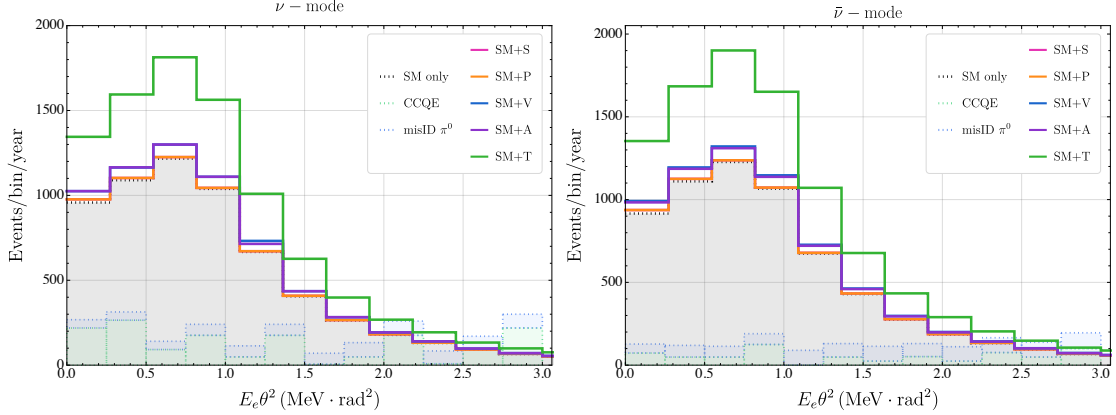


Figure 4. Expected distributions of the variable $x \equiv E_e \theta_e^2$ for the DUNE ND on-axis configuration with one year of exposure, shown separately for both the neutrino (left) and antineutrino (right) modes. The shaded regions below the dotted lines denote the SM background from $\nu(\bar{\nu})-e^-$ elastic scattering and the subdominant backgrounds from CCQE and mis-identified π^0 events. The colored solid lines are for the total events including the NP signal contribution for the five Lorentz structures (scalar, pseudoscalar, vector, axial-vector, and tensor). We have taken the benchmark values of $m_\chi = 10$ MeV and $\Lambda_{i,e} = 650$ GeV for all the NP cases.

parameters $\alpha_{1,2}$ are for the flux ($\sigma_{\alpha_1} = 5\%$) and background ($\sigma_{\alpha_2} = 10\%$) normalization uncertainties, respectively [89]. The expected DUNE ND sensitivities of m_χ and $\Lambda_{i,e}$ for the four-fermion interactions in Eq. (2.1) are derived by minimizing the χ^2 function with respect to both the nuisance parameters α_i and the NP parameters.

4 Hadronic absorption operators

We obtain in Sec. 4.1 the exclusion limits of COHERENT and CONUS+ on the effective cutoff scales $\Lambda_{i,N}$ for the couplings of neutrino and dark particles to nucleons, as functions of the dark particle mass m_χ . In Sec. 4.2, we collect the other existing constraints on the cutoff scales $\Lambda_{i,N}$ that are comparable to or more stringent than the COHERENT and CONUS+ limits. For the sake of completeness, all other weaker limits are listed in Sec. 4.3.

4.1 Exclusion limits from COHERENT and CONUS+

Based on the analysis in Sec. 3, the excluded regions by the current COHERENT and CONUS+ data are shown as the blue and green shaded regions in Fig. 5. The five panels are for the scalar, pseudoscalar, vector, axial-vector and tensor coupling forms, respectively. As stated in Sec. 2.3, the dark particle mass ranges accessible in CE ν NS experiments are primarily determined by the energies of the neutrino sources employed. For the CONUS+ experiment, which use reactor antineutrinos with typical energies of a few MeV, the exclusion limits extend only up to $m_\chi \lesssim \mathcal{O}(10)$ MeV. In comparison, the COHERENT experiment is based on a spallation neutron source, producing neutrinos with energies up to several tens of MeV. Consequently, the excluded dark particle mass range can be extended to $m_\chi \lesssim \mathcal{O}(50)$ MeV.

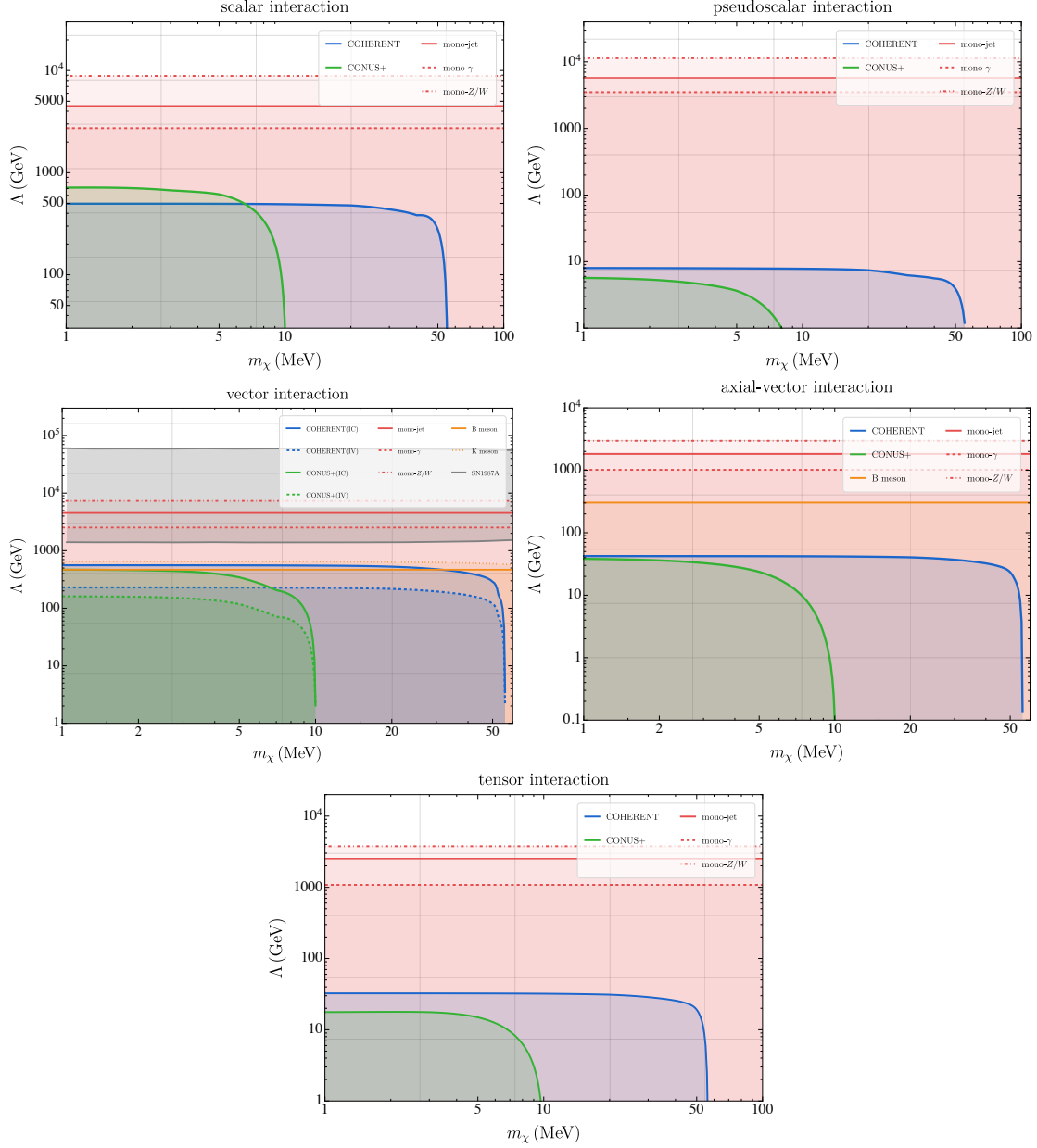


Figure 5. The 90% C.L. limits on the dark particle mass m_χ and the cutoff scales $\Lambda_{i,N}$ from the current COHERENT (shaded blue) and CONUS+ (shaded green) data, for all the five Lorentz structures of scalar (top left), pseudoscalar (top right), vector (middle left), axial-vector (middle right) and tensor (bottom) couplings. In the middle left panel, the limits for the IV vector couplings are indicated by the regions below the dashed blue and green lines. Also shown are the limits from the LHC mono-jet, mono- γ and mono- Z/W data [13], the FCNC B and K meson decays [69] and the SN1987A observations [81].

Let us now collect the exclusion limits on the cutoff scales $\Lambda_{i,N}$ for the different Lorentz structures of the effective interactions.

- For the scalar interaction, both COHERENT and CONUS+ benefit from the coherent

enhancement associated with the spin-independent coupling in the neutrino-nucleus scattering process. The exclusion limit from COHERENT reaches $\Lambda_{S,N} \simeq 450$ GeV, while CONUS+, due to its lower recoil energy threshold and operation deep in the fully coherent regime, provides a stronger constraint of $\Lambda_{S,N} \simeq 692$ GeV, as seen in the top left panel of Fig. 5.

- In contrast, the pseudoscalar interaction has the strongest suppression in CE ν NS experiments, as presented in the top-right panel of Fig. 5. The corresponding exclusion limits are only $\Lambda_{P,N} \simeq 8$ GeV for COHERENT and $\Lambda_{P,N} \simeq 6$ GeV for CONUS+, nearly two orders of magnitude weaker than those for scalar interactions. This severe reduction originates from both the momentum and spin suppressions that are inherent in the non-relativistic nuclear scatterings for a pseudoscalar coupling.
- For the vector coupling, the exclusion limits in the IC scenario are comparable to those of scalar interactions. COHERENT and CONUS+ yield exclusion limits of $\Lambda_{V,N}^{\text{IC}} \simeq 486$ GeV and $\Lambda_{V,N}^{\text{IC}} \simeq 388$ GeV, respectively, as indicated by the dashed blue and green lines in the middle-left panel of Fig. 5. This reflects the coherent enhancement of vector currents in nuclear targets.

In the IV scenario with $\Lambda_{V,p} = -\Lambda_{V,n}$, the effective nuclear coupling scales with neutron excess ($Z-N$), leading to severe suppression. The exclusion limits decrease to $\Lambda_{V,N}^{\text{IV}} \simeq 200$ GeV for COHERENT and $\Lambda_{V,N}^{\text{IV}} \simeq 133$ GeV for CONUS+, respectively, which are depicted as the dotted blue and green lines in the middle-left panel of Fig. 5. This behavior demonstrates the strong dependence of CE ν NS constraints on the nuclear composition of the detector material in isospin relevant scenarios.

- The axial-vector and tensor interactions are also to some extent suppressed due to their dependence on the nuclear spin, as seen in the middle right and bottom panels of Fig. 5. The exclusion limits obtained by COHERENT are $\Lambda_{A,N} \simeq 44$ GeV and $\Lambda_{T,N} \simeq 25$ GeV, while CONUS+ yields $\Lambda_{A,N} \simeq 38$ GeV and $\Lambda_{T,N} \simeq 18$ GeV, respectively. These results demonstrate the intrinsic disadvantage of spin-dependent interactions in CE ν NS experiments dominated by nuclei with small spins.

As clearly seen in the panels of Fig. 5, the CE ν NS experiments exhibit a clear hierarchy among different Lorentz structures: the scalar and IC vector interactions have the strongest exclusion limits, whereas the pseudoscalar, axial-vector, and tensor interactions are significantly suppressed. As we will see in Sec. 5, this pattern stands in sharp contrast to the results provided by the neutrino-electron scattering at DUNE ND, underscoring the complementarity between these two classes of experiments.

It should be emphasized that the parameter space probed by COHERENT and CONUS+ has already been constrained by the existing LHC 13 TeV data [13]. The constraints on the cutoff scales $\Lambda_{i,N}$ can be significantly improved by the future COHERENT and CONUS+ data, which however, are still below the current LHC limits [8] to be detailed below. As a result, the CE ν NS bounds presented here do not constitute the primary discovery reach of this work, but instead serve as important and realistic benchmarks that provide complementary information to the DUNE ND results.

4.2 Limits from LHC data, FCNC meson decays and SN1987A

The leading constraints on the effective interactions in Eq. (2.1) for nucleon are from the direct production of dark particles at the LHC, the FCNC meson decays, and the supernova explosion.

LHC limits The effective operators involving nucleons are severely constrained by the existing LHC data. To adopt the LHC constraints, we need to correlate the effective couplings of nucleons in Eq. (2.1) to that of quarks:

$$\mathcal{L}_{\text{eff},q} = \sum_i \frac{1}{\Lambda_{i,q}^2} (\bar{\chi} \Gamma^i P_L \nu) (\bar{q} \Gamma_i q) + \text{h.c.}, \quad (4.1)$$

with $\Lambda_{i,q}$ the corresponding cutoff scales. As the couplings involving gluons are always at the 1-loop or higher order, for simplicity we consider here only the couplings with quarks. The cutoff scales $\Lambda_{i,q}$ are correlated with $\Lambda_{i,N}$ through the form factors \mathcal{F}_i via the relation [13, 117–120]

$$\mathcal{F}_i (\bar{N} \Gamma_i N) \simeq (\bar{q} \Gamma_i q). \quad (4.2)$$

This implies that

$$\Lambda_{i,N}^2 \simeq \mathcal{F}_i \Lambda_{i,q}^2, \quad \text{with } i = S, P, V, A, T. \quad (4.3)$$

More details can be found in Appendix B.

Neutrinos, DM and other invisible particles can be produced at the high energy hadron colliders, e.g. from their interactions with quarks, and emerge as missing transverse energy \cancel{E}_T at the detectors [15–17]. The main LHC constraints are from the processes of $q\bar{q} \rightarrow X + \nu\bar{\chi}$, with $X = \text{jet}, \gamma$ and Z/W . This corresponds to the mono-jet [157, 158], mono- γ [159] and mono- Z/W [160–162] signals at the LHC, respectively. All these analysis are based on the simplified DM models with a heavy mediator. These LHC limits have been re-interpreted and recast onto the EFT couplings of quarks in Eq. (4.1) [13]. The resultant constraints on the cutoff scales $\Lambda_{i,N}$ at the nucleon level are presented as the red lines with shaded regions in Fig. 5. It is very clear that for all the five Lorentz structures the current LHC limits are much more stringent than the current constraints from COHERENT and CONUS+.

FCNC meson decay limits The couplings of DM χ with quarks in the form of

$$(\bar{\chi} \Gamma^i \chi)(\bar{q} \Gamma_i q), \quad (4.4)$$

could induce the exotic FCNC decays, e.g. $d_j \rightarrow d_i \chi \bar{\chi}$. Such processes are constrained by the precise data of the meson decays $B \rightarrow K^{(*)} \nu \bar{\nu}$, $B \rightarrow \pi \nu \bar{\nu}$, $\rho \nu \bar{\nu}$ and $K \rightarrow \pi \nu \bar{\nu}$ [37, 40, 45, 63, 68–70]. Here we adopt the recent FCNC limits from Ref. [69]. When we recast these limits onto the channels $d_j \rightarrow d_i \nu \bar{\chi}$ induced by the couplings in Eq. (2.1), the corresponding limits are in principle different from the limits on $d_j \rightarrow d_i \chi \bar{\chi}$, depending on the mass m_χ . For the mass range of $m_\chi \lesssim 100$ MeV of interest in this paper, which is much smaller than the Kaon and B meson masses, the difference is insignificant and can be safely neglected. Constraints are derived on the products of vector and axial-vector quark

Table 1. The 90% C.L. limits on the cutoff scales $\Lambda_{i,N}$ in Eq. (2.1) from the current COHERENT and CONUS+ data. Also shown are the existing limits from the LHC mono-jet, mono- γ and mono- Z/W data, FCNC meson decay and SN1987A observations. All the limits are for the mass of $m_\chi \rightarrow 0$, and in unit of GeV.

| int. | COHE- RENT | CONUS+ | LHC [13] | | | meson [69] | | SN1987A [81] |
|------|---------------|--------|-------------------|-------------------|-------------------|-------------------|-----|--------------|
| | | | mono-jet | mono- γ | mono- Z/W | B | K | |
| S | 450 | 710 | 4.5×10^3 | 2.7×10^3 | 8.8×10^3 | — | — | — |
| P | 8 | 6 | 5.8×10^3 | 3.5×10^3 | 1.1×10^4 | — | — | — |
| V | IC | 486 | 388 | 4.5×10^3 | 2.5×10^3 | 7.3×10^3 | 467 | 646 |
| | IV | 200 | 133 | — | — | — | — | — |
| A | 44 | 38 | 1.8×10^3 | 1.0×10^3 | 2.9×10^3 | 304 | — | — |
| T | 25 | 18 | 2.5×10^3 | 1.1×10^3 | 3.8×10^3 | — | — | — |

and dark sector couplings $g_q^V g_\chi^V$ and $g_q^A g_\chi^A$ from the rare B and K decays. For the heavy gauge boson Z' mediator with mass $m_{Z'}$, these bounds can be mapped onto the quark-level four-fermion operators in Eq. (4.4) with the corresponding effective quark-level cutoff scales $\Lambda_{i,q} \equiv m_{Z'} / \sqrt{g_f^i g_\chi^i}$ for $i = V, A$. In B meson decays, the channels $B^0 \rightarrow K^0 \nu \bar{\nu}$, $\pi^0 \nu \bar{\nu}$ and $B^0 \rightarrow K^{*0} \nu \bar{\nu}$ provide the most stringent constraints for the vector and axial-vector couplings, respectively. The kaon decay $K^+ \rightarrow \pi^+ \nu \bar{\nu}$ offers comparable constraints on the effective vector coupling. Following the same procedure procedure above, the limits on the quark-level couplings can be converted onto the constraints on the cutoff scales $\Lambda_{i,N}$ at the nucleon level. As seen in the middle-left and middle-right panels of Fig. 5, the B meson decays lead to the limits of $\Lambda_{V,N}^{\text{IC}} \gtrsim 467 \text{ GeV}$ and $\Lambda_{A,N} \gtrsim 304 \text{ GeV}$, while the K meson constraint is $\Lambda_{V,N}^{\text{IC}} \gtrsim 646 \text{ GeV}$.

Supernova limits The scattering process in Eq. (2.2b) could also occur in the supernova core. Therefore, the cutoff scales $\Lambda_{i,N}$ are tightly constrained by the supernova observations. In particular, copious of χ can be produced in the $\nu(\bar{\nu})$ -nucleon scattering in supernovae, and then escape from the stars. By requiring that the energy carried away by dark particles does not exceed a certain fraction of the total neutrino emission (the Raffelt cooling criterion) [163], very stringent constraints can be obtained for the mass range of $m_\chi \lesssim \mathcal{O}(100 \text{ MeV})$. The supernova cooling constraint on the IC vector coupling case have been recently obtained in Ref. [81]. Although the supernova limit in this paper is based on the assumption of χ being DM, it applies also to our case of χ being unstable dark particle instead of DM, as the decay length of χ is much larger than the typical size of supernova cores. It turns out the range of $1.5 \text{ TeV} \lesssim \Lambda_{V,N}^{\text{IC}} \lesssim 60 \text{ TeV}$ is excluded by the SN1987A data, which is presented as the gray shaded band in Fig. 5.

For the convenience of readers, the limits on the cutoff scales $\Lambda_{i,N}$ from the current COHERENT and CONUS+ data, and the existing LHC, meson and supernova limits above have been compiled together in Table 1. All these limits are for the light dark particle with vanishing mass $m_\chi \rightarrow 0$. It is transparent in this table that the current most stringent constraints are from the high-energy LHC data and the SN1987A observations.

4.3 Other weak constraints

In this subsection, we collect all the weak and inapplicable constraints on the effective couplings of neutrino and dark particle χ with nucleons in Eq. (2.1).

- **(Semi-)invisible quarkonium decays.** The searches of (semi-)invisible quarkonium decays at BaBar provide direct bounds on the quark-level process $q\bar{q} \rightarrow \chi\bar{\chi}$ and $q\bar{q} \rightarrow \chi\bar{\chi}\gamma$, which are complementary to the mono- X constraints at the LHC [43]. In particular, the BaBar collaboration reports the upper limits $\mathcal{B}(\Upsilon(1S) \rightarrow \text{invisible}) < 3 \times 10^{-4}$ and $\mathcal{B}(\Upsilon(3S) \rightarrow \gamma + \text{invisible}) < (0.7 \sim 31) \times 10^{-6}$, depending on the missing mass window. As in the case of FCNC meson decays in Sec. 4.2, these data can be used to constrain the channels of $q\bar{q} \rightarrow \nu\bar{\chi}$, $\nu\bar{\chi}\gamma$, which can arise from the couplings of neutrino and dark particle χ with the bottom quark. It turns out that $\Lambda \gtrsim \mathcal{O}(100) \text{ GeV}$.
- **Radiative Z and tauon decays.** The couplings in Eq. (2.1) contribute at the 1-loop order to the invisible decay of Z boson via the channels of $Z \rightarrow \nu\bar{\chi}$, $\chi\bar{\nu}$, which is quite similar to the effects of neutrino NSIs [51]. The corresponding limits on the cutoff scales are $\Lambda \gtrsim 200 \text{ GeV}$. The couplings of neutrinos (and the dark particle χ) with quarks induce extra 1-loop contributions to the decay of tauon $\tau \rightarrow \pi\nu(\pi\chi)$. However, limited by the precision of tauon data, the corresponding constraints are expected to be weaker [51].
- **DM direct detection.** The DM direct detection experiments provide an important platform for probing neutrino relevant NP. If χ is identified as the DM particle, the effective coupling in Eq. (2.1) could induce the absorption of DM in the direct detection experiments via the process of $\chi + \mathcal{N} \rightarrow \mathcal{N} + \nu$. Thanks to the low energy thresholds and large exposures of the DM direct detection experiments, the corresponding limits on the cutoff scales $\Lambda_{i,N}$ can reach $\mathcal{O}(\text{TeV})$ for the scalar and vector couplings [164–167]. However, such constraints do *not* apply to our case, with χ being an unstable particle.
- **Light mediator portal dark particle searches.** The dark particle χ can couple to the SM particles via a light mediator, e.g. a light scalar or a dark photon at or below the GeV. Then the light mediator can be produced from meson decays or at the fixed target experiments, and then decays into a pair of dark particles [71–76, 168–173]. However, the constraints from such processes can not be used to directly constrain the effective four-fermion couplings in Eq. (2.1). The dark particle χ can be pair-produced from the fixed target experiments, but the corresponding constraints are expected to be much weaker than the light mediator case.

5 Leptonic absorption operators

This section focuses mostly on the couplings of neutrinos and dark particle with electrons. The expected sensitivities at the DUNE ND are obtained in Sec. 5.1. The relevant con-

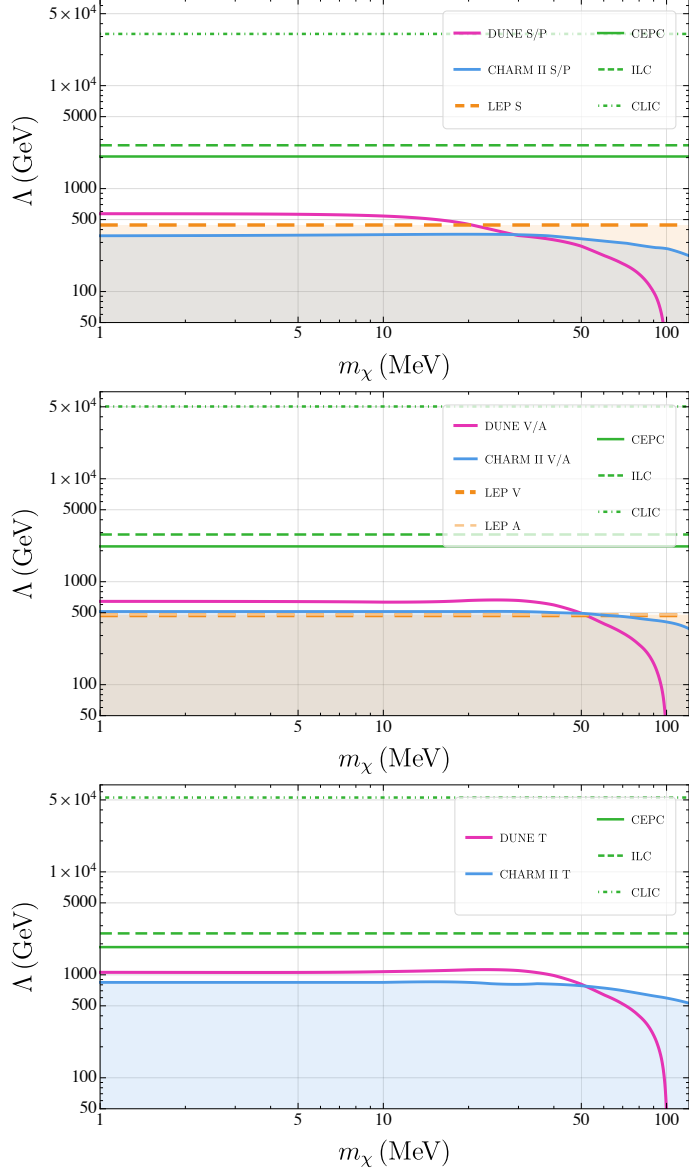


Figure 6. The 90% C.L. sensitivities of DUNE ND to the dark particle mass m_χ and the cutoff scales $\Lambda_{i,e}$, for the scalar/pseudoscalar (top), vector/axial-vector (middle), and tensor (bottom) interactions, shown as the solid magenta curves. Also shown are the existing constraints from CHARM II [9] and LEP [20], which are depicted as the shaded regions below the solid blue lines and dashed orange lines, respectively. The green lines correspond to the projected sensitivities of future lepton colliders [18]. See text for more details.

straints from the current CHARM II and LEP data and the prospects at future high-energy lepton colliders are given in Sec. 5.2. Some other weaker constraints are collected in Sec. 5.3.

5.1 The sensitivities at DUNE ND

The typical energy of the neutrino beam in DUNE is at the GeV scale. As stated in Sec. 2.3, the mass m_χ can be probed up to $\mathcal{O}(100 \text{ MeV})$ at the DUNE ND, significantly higher than

that of low-energy neutrino experiments based on reactors or spallation sources. Furthermore, comparing with the neutrino-nucleus scattering, the neutrino-electron scattering does not involve nuclear structure effects and there is no additional suppression caused by the nuclear spin or isospin structure. Benefiting from the high POT of DUNE and the well controlled background environment, the sensitivities of $\Lambda_{i,e}$ at the DUNE ND are comparable to or significantly higher than the limits on $\Lambda_{i,N}$ from COHERENT and CONUS+ in Sec. 4, depending on the Lorentz structures involved. Based on the analysis in Sec. 3.3, the resultant sensitivity of DUNE ND to the effective cutoff scales $\Lambda_{i,e}$ are shown as the solid magenta lines in Fig. 6, as functions of m_χ . The top, middle and bottom panels are for the scalar (pseudoscalar), vector (axial-vector) and tensor couplings, respectively. All sensitivities are shown at the 90% C.L..

- At DUNE ND, the recoil electrons in the (anti)neutrino-electron scattering are typically relativistic. Consequently, unlike in low-energy CE ν NS measurements such as COHERENT and CONUS+ experiments, there is no suppression behavior of the pseudoscalar interaction. In particular, the projected sensitivities for the scalar and pseudoscalar cases almost coincide over the entire dark particle mass range, and are represented by the same solid magenta curve in the top panel of Fig. 6, reaching $\Lambda_{S(P),e} \simeq 560$ GeV up to 560 GeV.
- Similarly, the sensitivities for the vector and axial-vector interactions are nearly identical, with $\Lambda_{V(A),e} \simeq 650$ GeV, as shown in the middle panel of Fig. 6. This indicates that in the energy range and detection channels of DUNE ND considered here, these operators lead to essentially the same sensitivity.
- As seen in the bottom panel of Fig. 6, the tensor interaction gives the strongest sensitivity throughout the mass range, with the corresponding effective cutoff scale reaching $\Lambda_{T,e} \simeq 1.07$ TeV.
- When the dark particle mass approaches the kinematic threshold, $m_\chi \sim 100$ MeV, the sensitivities for all the operators decrease rapidly due to kinematics.

For the convenience of readers, the sensitivities to $\Lambda_{i,e}$ in the limit $m_\chi \rightarrow 0$ for all the five Lorentz structures at DUNE ND are collected in Table 2.

There are some studies of the sensitivities of DUNE ND in simplified models with light mediators [89]. Our estimates in the framework of effective dimension-6 couplings in Eq. (2.1) correspond to the heavy mediator limit, analogous to the Fermi theory description of the weak interaction. While the analysis of Ref. [89] is performed in the light mediator framework with an explicit propagator dependence, it is nevertheless instructive to compare the order-of-magnitude sensitivities of these two approaches. Formally, the heavy mediator EFT can be related to simplified models through the correspondence,

$$\frac{1}{\Lambda^2} \sim \frac{g_{\text{eff}}^2}{m_{\text{med}}^2}, \quad (5.1)$$

Table 2. Expected sensitivity of the cutoff scales $\Lambda_{i,e}$ in Eq. (2.1) at the 90% C.L. for the DUNE ND. Also shown are the current CHARM II and LEP limits and prospects at future high-energy lepton colliders. The limits and prospects are for the dark particle mass $m_\chi \rightarrow 0$, and are given in GeV. See text and Fig. 6 for more details.

| int. | DUNE | CHARM II [9] | LEP [20] | future lepton colliders [18] | | |
|------|------|--------------|----------|------------------------------|-------------------|-------------------|
| | | | | CEPC | ILC | CLIC |
| S/P | 560 | 348 | 440 | 2.0×10^3 | 2.6×10^3 | 3.2×10^4 |
| V | 650 | 493 | 470 | 2.2×10^3 | 2.8×10^3 | 5.0×10^4 |
| A | | | 480 | | | |
| T | 1070 | 779 | — | 1.8×10^3 | 2.5×10^3 | 5.3×10^4 |

with g_{eff} being the effective coupling involved. This correspondence is valid only in the limit of $m_{\text{med}} \gg |\mathbf{q}|$. At the DUNE experiment, the typical momentum transfer in neutrino-electron scattering is $|\mathbf{q}| \sim \mathcal{O}(10-50)$ MeV. The projected sensitivities for light mediators over a range of benchmark parameters are obtained in Ref. [89]. Taking, for instance, the benchmark scenario with $m_\chi = 0.1 m_{\text{med}}$ (with m_{med} being the mediator mass), we find that the sensitivities to the cutoff scales $\Lambda_{i,e}$ obtained in this work are consistent with the corresponding sensitivities of the effective coupling g_{eff} at the DUNE ND in Ref. [89].

5.2 CHARM II and LEP limits and prospects at future lepton colliders

The cutoff scales $\Lambda_{i,e}$ are constrained by the $\nu(\bar{\nu})$ - e^- scattering at the CHARM II experiment. Following the analysis of Ref. [9], the existing CHARM II data yield the following 90% C.L. lower bounds in the limit $m_\chi \rightarrow 0$: $\Lambda_{S(P),e} \gtrsim 348$ GeV, $\Lambda_{V(A),e} \gtrsim 493$ GeV and $\Lambda_{T,e} \gtrsim 779$ GeV. These CHARM II bounds are shown as the blue curves in Fig. 6 and are summarized in Table 2.

The effective couplings of neutrinos and χ with electrons are also constrained by the existing LEP data. The operators of electrons and DM χ

$$\mathcal{O}_i = (\bar{\chi} \Gamma^i \chi)(\bar{e} \Gamma_i e) \quad (5.2)$$

can induce mono- γ signals at high-energy e^+e^- colliders. The existing LEP data have excluded the cutoff scales $\Lambda_{i,e} \lesssim 440$ GeV, 470 GeV and 480 GeV for the Lorentz structures of scalar, vector and axial-vector couplings [20]. Recast onto the couplings in Eq. (2.1), the limits are expected to be the same, as the mass m_χ is too much lower than the energy scale of LEP. The LEP limits are shown as the shaded regions below the orange dashed lines in Fig. 6 and are also collected in Table 2. As clearly seen in Fig. 6, the DUNE ND can probe large cutoff scales $\Lambda_{i,e}$ beyond the CHARM II and LEP limits, for dark particle mass m_χ up to roughly 50 MeV.

The prospects for probing $\Lambda_{i,e}$ can be significantly improved at the future high-energy lepton colliders, as detailed in Ref. [18] (see also Ref. [29] for studies of the operator (5.2) at future lepton colliders). Early studies of the mono- γ channel at the ILC can be found in Ref. [23], which estimates a reach of $\Lambda \sim (1 \sim 1.2)$ TeV at $\sqrt{s} = 250$ GeV

and $\Lambda \sim (3 \sim 4) \text{ TeV}$ at $\sqrt{s} = 1 \text{ TeV}$ with polarized beams. Related model-independent analyses of radiative dark particle pair production, $e^+e^- \rightarrow \chi\bar{\chi}\gamma$, were also performed in Refs. [21, 22]. At the future high-energy e^+e^- colliders, the most sensitive probes of the effective couplings in Eq. (2.1) involving electrons are in the channels with final states of mono- γ and $e^+e^- + \cancel{E}_T$. The corresponding sensitivities of $\Lambda_{i,e}$ depend largely on the center-of-mass energy \sqrt{s} and the integrated luminosity. Combining both channels, it is found that $\Lambda_{i,e}$ can be probed up to $\sim 2 \text{ TeV}$ at the CEPC with $\sqrt{s} = 240 \text{ GeV}$ and a luminosity of 5.6 ab^{-1} . At the ILC with $\sqrt{s} = 500 \text{ GeV}$ and 4 ab^{-1} and the CLIC with $\sqrt{s} = 3 \text{ TeV}$ and 5 ab^{-1} , the sensitivities of $\Lambda_{i,e}$ can be improved up to $\sim 2.5 \text{ TeV}$ and $\sim 30 \text{ TeV}$. Conservatively, all the beams are assumed to be unpolarized. These CEPC, ILC and CLIC prospects are presented in Fig. 6 as the solid, dashed and dot-dashed green lines, respectively. The corresponding specific values of $\Lambda_{i,e}$ are collected in Table 2.

5.3 Other weak constraints

We now list some other constraints that are relatively weak or not applicable to our framework.

- **Dark particle searches at B -factories.** The sub-GeV dark particles can also be searched for at the B -factories via the mono-photon process of $e^+e^- \rightarrow \gamma\chi\bar{\chi}$. However, with an integrated luminosity of 50 ab^{-1} at Belle II, the cutoff scales $\Lambda_{i,e}$ can only be probed up to roughly 300 GeV , significantly lower than the current LEP limits [31, 35] and the prospects at future high-energy lepton colliders [18, 21–23, 29].
- **Dark particle searches at beam-dump experiments.** Given the operator in Eq. (5.2), dark particles can be pair-produced at the electron beam dump experiments via the process of $e^- + \gamma \rightarrow e^- + \chi + \bar{\chi}$, where the photon is emitted from the target nuclei. The constraints from the existing NA64 data are rather weak, with $\Lambda_i \gtrsim 10 \text{ GeV}$ [31].
- **Dark particle with electromagnetic form factors.** There have been studies of dark particles with electromagnetic form factors, which will induce the pair production of dark particle χ at the electron beam experiments such as BaBar, NA64 and mQ, mediated by a virtual photon [32]. Re-interpreting onto the cutoff scales $\Lambda_{i,e}$ is constrained up to the scale of 200 GeV . Future fixed-target experiments such as LDMX and BDX can probe the magnetic dipole moment $\mu_\chi \sim 10^{-6} \mu_B$, which corresponds to $\Lambda \gtrsim \mathcal{O}(1 \text{ TeV})$.
- **Low-energy neutrino experiments.** The dark particle χ can be produced at the low-energy neutrino experiments TEXONO, and Borexino. However, these experiments are only sensitive to the mass range of $m_\chi \lesssim 1 \text{ MeV}$ [9].
- **Light mediator portal dark particle searches.** Dark particles can couple to electrons via a light mediator [33, 34, 65, 153, 169, 174–182]. However, as discussed in Sec. 4.3, the constraints can not be directly recast onto the cutoff scales in Eq. (2.1).

- **Four-body meson and tauon decays.** The couplings of neutrinos and dark particle χ with electron will induce some exotic charged lepton and meson decays, e.g. the four-body tauon decay $\tau^- \rightarrow \pi^- e^+ e^- \chi$ and the meson decay $\pi^+, K^+ \rightarrow \ell^+ e^+ e^- \chi$, with the $e^+ e^-$ pair emitted from the neutrino line. However, these channels are highly suppressed by the phase space, and the limits from experimental measurements in the channels $\tau^- \rightarrow \pi^- e^+ e^- \nu_\tau$ [183], $\pi^+ \rightarrow e^+ e^+ e^- \nu_e$ [184] and $K^+ \rightarrow \ell^+ e^+ e^- \nu_\ell$ ($\ell = e, \mu$) [185] are expected to be rather weak.
Similarly, the four-body meson decays $\pi^-, K^- \rightarrow e^- \nu(\nu\bar{\chi}, \chi\bar{\nu})$ are also possible, with the $(\nu\bar{\chi})$ or $(\chi\bar{\nu})$ pair connected to the final-state electron line. In the limit of $m_\chi \rightarrow 0$, the corresponding signals look quite similar as the decays $\pi^-, K^- \rightarrow e^- \nu\nu\bar{\nu}$, which can be induced by neutrino self-interactions [52–54]. However, the corresponding limits from the data of $\pi^+ \rightarrow e^+ \nu_e \nu\bar{\nu}$ [186] and $K^+ \rightarrow e^+ \nu_e \nu\bar{\nu}$ [187] are also very weak (cf. the relevant discussions in Ref. [7]).
- **Five-body muon and tauon decays.** The operator in Eq. (2.1) will induce the five-body muon decays $\mu^- \rightarrow e^- e^+ e^- (\nu_\mu \bar{\chi}, \chi \bar{\nu}_e)$ and tauon decays $\tau^- \rightarrow \ell^- e^+ e^- (\nu\bar{\chi}, \chi\bar{\nu})$ (with $\ell = e, \mu$), with the $e^+ e^-$ pair emitted from the (anti)neutrino line. These channels are constrained by measurements of the SM processes $\mu^- \rightarrow e^- \nu_\mu \bar{\nu}_e e^+ e^-$ [188] and $\tau^- \rightarrow \ell^- e^+ e^- \nu\bar{\nu}$ [189]. With extra neutrinos and the dark particle χ emitting from the electron line in the final state, there are also the five-body charged lepton decays $\mu, \tau \rightarrow e\nu\bar{\nu}(\nu\bar{\chi}, \chi\bar{\nu})$, which look quite similar to the SM processes $\mu, \tau \rightarrow e\nu\bar{\nu}$ and the four-body decays $\mu, \tau \rightarrow e\nu\bar{\nu}\phi$ with ϕ a neutrinoophilic scalar [190–192]. However, the corresponding limits in these channels are expected to be very weak due to phase space suppression.
- **Four-body W boson decays.** There might be the rare decay of $W \rightarrow e\nu(\nu\bar{\chi}, \chi\bar{\nu})$ induced by the couplings in Eq. (2.1), with (anti)neutrino and $\chi(\bar{\chi})$ emitted from the electron line. These decay channels are quite similar to $W \rightarrow e\nu\nu\bar{\nu}$, which can be induced by neutrino self-interactions [52, 55]. However, suppressed again by the four-body phase space, the constraints from the W data are rather weak [193].
- **Radiative Z, W and meson decays.** At the 1-loop order, the couplings of neutrinos and dark particle with electrons in Eq. (2.1) induce the exotic radiative decays $Z \rightarrow \nu\bar{\chi}, \chi\bar{\nu}$ [51]. The precision measurements of the invisible partial width of Z boson set constraints on the cutoff scales $\Lambda_{i,e} \gtrsim \mathcal{O}(100 \text{ GeV})$. The precision measurements of $W \rightarrow e\nu$ can also be used to constrain the decay channel of $W \rightarrow e\chi$, which is induced by the couplings of neutrinos and dark particle χ with electrons [51], but the corresponding precision are to some extent lower than that from Z data, which leads to weaker constraints on the cutoff scales [193]. The couplings in Eq. (2.1) could also induce the radiative exotic meson decay $M^- \rightarrow e^- \bar{\chi}$, which, however, is highly suppressed by the loop factor and electron mass (cf. the 1-loop corrections to the meson decays $M^- \rightarrow e^- \bar{\nu}$ in Ref. [194]).

- **DM direct detection.** In the case of $m_\chi < 1$ MeV, χ could play as decaying DM, and induce electron recoil signals via the process of $\chi + e^- \rightarrow e^- + \nu$ in the DM direct detection experiments [10, 11]. However, the corresponding stringent limits from DM direct detection experiments [195–197] are not applicable to the case of $m_\chi > 1$ MeV, as a result of the rapid decay of χ .
- **Supernova observations.** The dark particle can be produced in the supernova core via the process $\nu + e \rightarrow \chi + e$. Therefore, the effective couplings in Eq. (2.1) for electrons are constrained by the supernova observations, e.g. from the cooling of SN1987A [81]. However, for $m_\chi > 2m_e$, χ could decay via $\chi \rightarrow \nu e^+ e^-$ inside the supernova core (cf. Eq. (2.7)) and weaken or invalidate the supernova cooling constraints in some regions of the parameter space. The supernova limits in Ref. [81] are therefore only for $m_\chi < 1$ MeV, not applicable to the mass range of $m_\chi > 1$ MeV in this paper.

6 Conclusion

In this work, we have performed a model-independent analysis of the effective couplings of neutrino, dark particle χ with nucleons or electrons at some representative neutrino scattering experiments, for all the five possible Lorentz structures of scalar, pseudoscalar, vector, axial-vector and tensor interactions. For the hadronic absorption operators, the current COHERENT and CONUS+ data could exclude the cutoff scales $\Lambda_{i,N}$ up to the scale of few hundreds of GeV, less stringent than the existing LHC data and SN1987A observations (cf. Fig. 5 and Table 1). However, for the leptonic absorption operators, the cutoff scales $\Lambda_{i,e}$ for couplings with electrons can be probed up to ~ 1 TeV at the DUNE ND, with the dark particle mass m_χ up to ~ 100 MeV, depending to some extent on the Lorentz structure. The DUNE ND sensitivities are beyond the current CHARM II and LEP limits (cf. Fig. 6 and Table 2).

Acknowledgments

The authors would like to thank Xiao-Dong Ma for useful discussions. The work of RF and YZ is supported by the National Natural Science Foundation of China (NSFC) under Grant No. 12175039. The work of SFG is supported by the National NSFC under the Grant No. of 12375101 and 12425506. This work is also supported by State Key Laboratory of Dark Matter Physics and the Fundamental Research Funds for the Central Universities.

A Weak nuclear form factor and spin structure functions

In this appendix we collect the nuclear physics inputs used in Eq. (2.3), namely the weak nuclear form factor $F_W(|\mathbf{q}|^2)$ and the spin structure functions $\tilde{S}^T(|\mathbf{q}|^2)$ and $\tilde{S}^L(|\mathbf{q}|^2)$, with the three-momentum transfer $|\mathbf{q}|^2 \simeq 2m_N T_N$.

The weak nuclear form factor $F_W(|\mathbf{q}|^2)$ accounts for the finite size and nuclear physics effects of the target nucleus. Following Refs. [198, 199], we adopt the Klein-Nystrand

parametrization,

$$F_W(|\mathbf{q}|^2) = \frac{3 j_1(|\mathbf{q}|R_A)}{|\mathbf{q}|R_A (1 + a_k^2 |\mathbf{q}|^2)}, \quad (\text{A.1})$$

where $j_1(x) = \sin x/x^2 - \cos x/x$ is the spherical Bessel function of order one, $R_A = 1.23 \text{ fm}^{1/3}$ is the effective nuclear radius, and $a_k = 0.7 \text{ fm}$ smears the nuclear surface.

Note that $\tilde{S}^T(|\mathbf{q}|^2)$ and $\tilde{S}^L(|\mathbf{q}|^2)$ are the transverse and longitudinal nuclear spin structure functions, respectively, which are relevant to the axial-vector and tensor interactions. We follow the standard multipole decomposition of the nuclear current and encode nuclear structure effects in spin structure functions, as commonly adopted in studies of spin-dependent neutrino-nucleus scattering [199, 200]. It is convenient to define

$$S_X^\kappa(|\mathbf{q}|^2) = (g_X^0)^2 S_{00}^\kappa(|\mathbf{q}|^2) + g_X^0 g_X^1 S_{01}^\kappa(|\mathbf{q}|^2) + (g_X^1)^2 S_{11}^\kappa(|\mathbf{q}|^2), \quad (\text{A.2})$$

where $X = A, T$ stands for the interaction type, $\kappa = \mathcal{T}, \mathcal{L}$ denotes the transverse (\mathcal{T}) or longitudinal (\mathcal{L}) component, and S_{ij}^κ are the nuclear spin response functions depending on the target nucleus [200, 201]. The couplings g_X^0 and g_X^1 are the isoscalar and isovector combinations of the proton and neutron couplings:

$$g_X^0 = \frac{g_X^p + g_X^n}{2}, \quad g_X^1 = \frac{g_X^p - g_X^n}{2}, \quad (\text{A.3})$$

with $g_X^{p,n}$ the effective proton and neutron couplings, respectively, for the corresponding current X .

B Nucleon form factors

To quantitatively establish the correspondence between the quark level and nucleon level cutoff scales in Sec. 4.2, we adopt the nucleon form factors in Refs. [13, 120]. For the low-energy scattering processes of interest, we take the leading contribution in the limit of vanishing momentum transfer, i.e. $q^2 \simeq 0$. Assuming flavor universal couplings to the light quarks $q = u, d, s$ and isospin conservation, the conversion factors \mathcal{F}_i introduced above can be written as

$$\mathcal{F}_i = \sum_{q=u,d,s} \mathcal{F}_i^{q/N}, \quad (\text{B.1})$$

where $\mathcal{F}_i^{q/N}$ are defined through the nucleon matrix elements of the corresponding quark bilinears.

Using the conventions and numerical inputs of Ref. [13], the conversion factors for the five Lorentz structures are given by

$$\mathcal{F}_S \equiv \sum_{q=u,d,s} \frac{\sigma_q^N}{m_q} \simeq 3.90, \quad (\text{B.2a})$$

$$\mathcal{F}_P \equiv \sum_{q=u,d,s} \frac{F_P^{q/N}(0)}{m_q} \simeq 6.43, \quad (\text{B.2b})$$

$$\mathcal{F}_V \equiv \sum_{q=u,d,s} F_1^{q/N}(0) = 3, \quad (\text{B.2c})$$

$$\mathcal{F}_A \equiv \sum_{q=u,d,s} \Delta q^N \simeq 0.49, \quad (\text{B.2d})$$

$$\mathcal{F}_T \equiv \sum_{q=u,d,s} g_T^{q/N} \simeq 0.59, \quad (\text{B.2e})$$

where σ_q^N denotes the nucleon sigma terms, Δq^N is the axial-vector spin fractions, and $g_T^{q/N}$ is the tensor charges. All numerical values are taken from Ref. [13] in the $\overline{\text{MS}}$ scheme at $\mu = 2 \text{ GeV}$.

References

- [1] **JUNO** Collaboration, Angel Abusleme et al., “*First measurement of reactor neutrino oscillations at JUNO*,” [\[arXiv:2511.14593\]](https://arxiv.org/abs/2511.14593) [hep-ex].
- [2] Mohammad Sajjad Athar et al., “*Status and perspectives of neutrino physics*,” *Prog. Part. Nucl. Phys.* **124** (2022) 103947, [\[arXiv:2111.07586\]](https://arxiv.org/abs/2111.07586) [hep-ph].
- [3] Gianfranco Bertone, Dan Hooper, and Joseph Silk, “*Particle dark matter: Evidence, candidates and constraints*,” *Phys. Rept.* **405** (2005) 279–390, [\[arXiv:hep-ph/0404175\]](https://arxiv.org/abs/hep-ph/0404175).
- [4] Gianfranco Bertone and Dan Hooper, “*History of dark matter*,” *Rev. Mod. Phys.* **90** no. 4, (2018) 045002, [\[arXiv:1605.04909\]](https://arxiv.org/abs/1605.04909) [astro-ph.CO].
- [5] Leszek Roszkowski, Enrico Maria Sessolo, and Sebastian Trojanowski, “*WIMP dark matter candidates and searches—current status and future prospects*,” *Rept. Prog. Phys.* **81** no. 6, (2018) 066201, [\[arXiv:1707.06277\]](https://arxiv.org/abs/1707.06277) [hep-ph].
- [6] Marco Cirelli, Alessandro Strumia, and Jure Zupan, “*Dark Matter*,” [\[arXiv:2406.01705\]](https://arxiv.org/abs/2406.01705) [hep-ph].
- [7] P. S. Bhupal Dev, Doojin Kim, Deepak Sathyam, Kuver Sinha, and Yongchao Zhang, “*New Constraints on Neutrino-Dark Matter Interactions: A Comprehensive Analysis*,” [\[arXiv:2507.01000\]](https://arxiv.org/abs/2507.01000) [hep-ph].
- [8] We-Fu Chang and Jiajun Liao, “*Constraints on light singlet fermion interactions from coherent elastic neutrino-nucleus scattering*,” *Phys. Rev. D* **102** no. 7, (2020) 075004, [\[arXiv:2002.10275\]](https://arxiv.org/abs/2002.10275) [hep-ph].
- [9] Zikang Chen, Tong Li, and Jiajun Liao, “*Constraints on general neutrino interactions with exotic fermion from neutrino-electron scattering experiments*,” *JHEP* **05** (2021) 131, [\[arXiv:2102.09784\]](https://arxiv.org/abs/2102.09784) [hep-ph].
- [10] Jeff A. Dror, Gilly Elor, Robert McGehee, and Tien-Tien Yu, “*Absorption of sub-MeV fermionic dark matter by electron targets*,” *Phys. Rev. D* **103** no. 3, (2021) 035001, [\[arXiv:2011.01940\]](https://arxiv.org/abs/2011.01940) [hep-ph]. [Erratum: Phys.Rev.D 105, 119903 (2022)].
- [11] Shao-Feng Ge, Xiao-Gang He, Xiao-Dong Ma, and Jie Sheng, “*Revisiting the fermionic dark matter absorption on electron target*,” *JHEP* **05** (2022) 191, [\[arXiv:2201.11497\]](https://arxiv.org/abs/2201.11497) [hep-ph].
- [12] Jeff A. Dror, Gilly Elor, and Robert McGehee, “*Directly Detecting Signals from Absorption of Fermionic Dark Matter*,” *Phys. Rev. Lett.* **124** no. 18, (2020) 18, [\[arXiv:1905.12635\]](https://arxiv.org/abs/1905.12635) [hep-ph].

- [13] Kai Ma, Shao-Feng Ge, Lin-Yun He, and Ning Zhou, “*Complementary search of fermionic absorption operators at hadron colliders and direct detection experiments*,” *Phys. Rev. D* **113** no. 1, (2026) 015027, [[arXiv:2405.16878](https://arxiv.org/abs/2405.16878) [hep-ph]].
- [14] Kai Ma and Lin-Yun He, “*Constraining gluonic contact interaction of a neutrino-philic dark fermion at hadron colliders and direct detection experiments*,” *Phys. Dark Univ.* **48** (2025) 101933, [[arXiv:2405.20890](https://arxiv.org/abs/2405.20890) [hep-ph]].
- [15] Felix Kahlhoefer, “*Review of LHC Dark Matter Searches*,” *Int. J. Mod. Phys. A* **32** no. 13, (2017) 1730006, [[arXiv:1702.02430](https://arxiv.org/abs/1702.02430) [hep-ph]].
- [16] Antonio Boveia and Caterina Doglioni, “*Dark Matter Searches at Colliders*,” *Ann. Rev. Nucl. Part. Sci.* **68** (2018) 429–459, [[arXiv:1810.12238](https://arxiv.org/abs/1810.12238) [hep-ex]].
- [17] G. Krnjaic et al., “*A Snowmass Whitepaper: Dark Matter Production at Intensity-Frontier Experiments*,” [[arXiv:2207.00597](https://arxiv.org/abs/2207.00597) [hep-ph]].
- [18] Shao-Feng Ge, Kai Ma, Xiao-Dong Ma, and Jie Sheng, “*Associated production of neutrino and dark fermion at future lepton colliders*,” *JHEP* **11** (2023) 190, [[arXiv:2306.00657](https://arxiv.org/abs/2306.00657) [hep-ph]].
- [19] Stefano Profumo, Kris Sigurdson, and Lorenzo Ubaldi, “*Can we discover multi-component WIMP dark matter?*,” *JCAP* **12** (2009) 016, [[arXiv:0907.4374](https://arxiv.org/abs/0907.4374) [hep-ph]].
- [20] Patrick J. Fox, Roni Harnik, Joachim Kopp, and Yuhsin Tsai, “*LEP Shines Light on Dark Matter*,” *Phys. Rev. D* **84** (2011) 014028, [[arXiv:1103.0240](https://arxiv.org/abs/1103.0240) [hep-ph]].
- [21] Christoph Bartels, Mikael Berggren, and Jenny List, “*Characterising WIMPs at a future e^+e^- Linear Collider*,” *Eur. Phys. J. C* **72** (2012) 2213, [[arXiv:1206.6639](https://arxiv.org/abs/1206.6639) [hep-ex]].
- [22] Herbert Dreiner, Moritz Huck, Michael Krämer, Daniel Schmeier, and Jamie Tattersall, “*Illuminating Dark Matter at the ILC*,” *Phys. Rev. D* **87** no. 7, (2013) 075015, [[arXiv:1211.2254](https://arxiv.org/abs/1211.2254) [hep-ph]].
- [23] Yoonseok John Chae and Maxim Perelstein, “*Dark Matter Search at a Linear Collider: Effective Operator Approach*,” *JHEP* **05** (2013) 138, [[arXiv:1211.4008](https://arxiv.org/abs/1211.4008) [hep-ph]].
- [24] Ayres Freitas and Susanne Westhoff, “*Leptophilic Dark Matter in Lepton Interactions at LEP and ILC*,” *JHEP* **10** (2014) 116, [[arXiv:1408.1959](https://arxiv.org/abs/1408.1959) [hep-ph]].
- [25] Enrico Bertuzzo, Cristian J. Caniu Barros, and Giovanni Grilli di Cortona, “*MeV Dark Matter: Model Independent Bounds*,” *JHEP* **09** (2017) 116, [[arXiv:1707.00725](https://arxiv.org/abs/1707.00725) [hep-ph]].
- [26] Moritz Habermehl, Mikael Berggren, and Jenny List, “*WIMP Dark Matter at the International Linear Collider*,” *Phys. Rev. D* **101** no. 7, (2020) 075053, [[arXiv:2001.03011](https://arxiv.org/abs/2001.03011) [hep-ex]].
- [27] Hrishabh Bharadwaj and Ashok Goyal, “*Effective Field Theory approach to lepto-philic self conjugate dark matter*,” *Chin. Phys. C* **45** no. 2, (2021) 023114, [[arXiv:2008.13621](https://arxiv.org/abs/2008.13621) [hep-ph]].
- [28] Jan Kalinowski, Wojciech Kotlarski, Krzysztof Mekala, Paweł Sopicki, and Aleksander Filip Zarnecki, “*Sensitivity of future linear e^+e^- colliders to processes of dark matter production with light mediator exchange*,” *Eur. Phys. J. C* **81** no. 10, (2021) 955, [[arXiv:2107.11194](https://arxiv.org/abs/2107.11194) [hep-ph]].
- [29] Saumyen Kundu, Atanu Guha, Prasanta Kumar Das, and P. S. Bhupal Dev, “*EFT analysis*

of leptophilic dark matter at future electron-positron colliders in the mono-photon and mono-Z channels,” *Phys. Rev. D* **107** no. 1, (2023) 015003, [[arXiv:2110.06903](https://arxiv.org/abs/2110.06903) [hep-ph]].

[30] Basabendu Barman, Subhaditya Bhattacharya, Sudhakantha Girmohanta, and Sahabub Jahedi, “*Effective Leptophilic WIMPs at the e^+e^- collider,*” *JHEP* **04** (2022) 146, [[arXiv:2109.10936](https://arxiv.org/abs/2109.10936) [hep-ph]].

[31] Jinhan Liang, Zuowei Liu, and Lan Yang, “*Probing sub-GeV leptophilic dark matter at Belle II and NA64,*” *JHEP* **05** (2022) 184, [[arXiv:2111.15533](https://arxiv.org/abs/2111.15533) [hep-ph]].

[32] Xiaoyong Chu, Josef Pradler, and Lukas Semmelrock, “*Light dark states with electromagnetic form factors,*” *Phys. Rev. D* **99** no. 1, (2019) 015040, [[arXiv:1811.04095](https://arxiv.org/abs/1811.04095) [hep-ph]].

[33] I. V. Voronchikhin and D. V. Kirpichnikov, “*Resonant probing spin-0 and spin-2 dark matter mediators with fixed target experiments,*” *Phys. Rev. D* **107** no. 11, (2023) 115034, [[arXiv:2304.14052](https://arxiv.org/abs/2304.14052) [hep-ph]].

[34] Kento Asai, Sho Iwamoto, Maxim Perelstein, Yasuhito Sakaki, and Daiki Ueda, “*Sub-GeV dark matter search at ILC beam dumps,*” *JHEP* **02** (2024) 129, [[arXiv:2301.03816](https://arxiv.org/abs/2301.03816) [hep-ph]].

[35] Jinhan Liang, Zuowei Liu, and Lan Yang, “*Search for strongly interacting dark matter at Belle II,*” *Phys. Rev. D* **109** no. 11, (2024) 115003, [[arXiv:2312.08970](https://arxiv.org/abs/2312.08970) [hep-ph]].

[36] Bob McElrath, “*Invisible quarkonium decays as a sensitive probe of dark matter,*” *Phys. Rev. D* **72** (2005) 103508, [[arXiv:hep-ph/0506151](https://arxiv.org/abs/hep-ph/0506151)].

[37] Pierre Fayet, “*Constraints on Light Dark Matter and U bosons, from psi, Upsilon, K+, pi0, eta and eta-prime decays,*” *Phys. Rev. D* **74** (2006) 054034, [[arXiv:hep-ph/0607318](https://arxiv.org/abs/hep-ph/0607318)].

[38] Pierre Fayet, “*U-boson production in e^+e^- annihilations, psi and Upsilon decays, and Light Dark Matter,*” *Phys. Rev. D* **75** (2007) 115017, [[arXiv:hep-ph/0702176](https://arxiv.org/abs/hep-ph/0702176)].

[39] H. K. Dreiner, S. Grab, Daniel Koschade, M. Kramer, Ben O’Leary, and Ulrich Langenfeld, “*Rare meson decays into very light neutralinos,*” *Phys. Rev. D* **80** (2009) 035018, [[arXiv:0905.2051](https://arxiv.org/abs/0905.2051) [hep-ph]].

[40] David McKeen, “*WIMPless Dark Matter and Meson Decays with Missing Energy,*” *Phys. Rev. D* **79** (2009) 114001, [[arXiv:0903.4982](https://arxiv.org/abs/0903.4982) [hep-ph]].

[41] Gagik K. Yeghiyan, “*Upsilon Decays into Light Scalar Dark Matter,*” *Phys. Rev. D* **80** (2009) 115019, [[arXiv:0909.4919](https://arxiv.org/abs/0909.4919) [hep-ph]].

[42] Andriy Badin and Alexey A Petrov, “*Searching for light Dark Matter in heavy meson decays,*” *Phys. Rev. D* **82** (2010) 034005, [[arXiv:1005.1277](https://arxiv.org/abs/1005.1277) [hep-ph]].

[43] Nicolas Fernandez, Jason Kumar, Ilsoo Seong, and Patrick Stengel, “*Complementary Constraints on Light Dark Matter from Heavy Quarkonium Decays,*” *Phys. Rev. D* **90** no. 1, (2014) 015029, [[arXiv:1404.6599](https://arxiv.org/abs/1404.6599) [hep-ph]].

[44] Nicolas Fernandez, Ilsoo Seong, and Patrick Stengel, “*Constraints on Light Dark Matter from Single-Photon Decays of Heavy Quarkonium,*” *Phys. Rev. D* **93** no. 5, (2016) 054023, [[arXiv:1511.03728](https://arxiv.org/abs/1511.03728) [hep-ph]].

[45] Luc Darmé, Sebastian A. R. Ellis, and Tevong You, “*Light Dark Sectors through the Fermion Portal,*” *JHEP* **07** (2020) 053, [[arXiv:2001.01490](https://arxiv.org/abs/2001.01490) [hep-ph]].

[46] Enrico Bertuzzo and Marco Taoso, “*Probing light dark scalars with future experiments*,” *JHEP* **03** (2021) 272, [[arXiv:2011.04735](https://arxiv.org/abs/2011.04735) [hep-ph]].

[47] Philip Schuster, Natalia Toro, and Kevin Zhou, “*Probing invisible vector meson decays with the NA64 and LDMX experiments*,” *Phys. Rev. D* **105** no. 3, (2022) 035036, [[arXiv:2112.02104](https://arxiv.org/abs/2112.02104) [hep-ph]].

[48] Tong Li, Xiao-Dong Ma, Michael A. Schmidt, and Rui-Jia Zhang, “*Implication of $J/\psi \rightarrow (\gamma +)$ invisible for the effective field theories of neutrino and dark matter*,” *Phys. Rev. D* **104** no. 3, (2021) 035024, [[arXiv:2104.01780](https://arxiv.org/abs/2104.01780) [hep-ph]].

[49] Alexey S. Zhevlakov, Dmitry V. Kirpichnikov, Sergei N. Gninenco, Sergey Kuleshov, and Valery E. Lyubovitskij, “*Probing invisible vector meson decay mode with the hadronic beam in the NA64 experiment at SPS CERN*,” *Phys. Rev. D* **108** no. 11, (2023) 115005, [[arXiv:2309.09347](https://arxiv.org/abs/2309.09347) [hep-ph]].

[50] S. N. Gninenco, N. V. Krasnikov, and V. A. Matveev, “*Search for $K_{S,L}$ oscillations and invisible decays into the dark sector at NA64*,” *Natural Sci. Rev.* **1** (2024) 5, [[arXiv:2501.09772](https://arxiv.org/abs/2501.09772) [hep-ph]].

[51] S. Davidson, C. Pena-Garay, N. Rius, and A. Santamaria, “*Present and future bounds on nonstandard neutrino interactions*,” *JHEP* **03** (2003) 011, [[arXiv:hep-ph/0302093](https://arxiv.org/abs/hep-ph/0302093)].

[52] Mikhail S. Bilenky and Arcadi Santamaria, “*’Secret’ neutrino interactions*,” in *Neutrino Mixing: Meeting in Honor of Samoil Bilenky’s 70th Birthday*, pp. 50–61. 8, 1999. [[arXiv:hep-ph/9908272](https://arxiv.org/abs/hep-ph/9908272)].

[53] D. Yu. Bardin, Samoil M. Bilenky, and B. Pontecorvo, “*On the ν - ν interaction*,” *Phys. Lett. B* **32** (1970) 121–124.

[54] Kevin J. Kelly and Yue Zhang, “*Mononeutrino at DUNE: New Signals from Neutrinoophilic Thermal Dark Matter*,” *Phys. Rev. D* **99** no. 5, (2019) 055034, [[arXiv:1901.01259](https://arxiv.org/abs/1901.01259) [hep-ph]].

[55] Mikhail S. Bilenky, Samoil M. Bilenky, and A. Santamaria, “*Invisible width of the Z boson and ’secret’ neutrino-neutrino interactions*,” *Phys. Lett. B* **301** (1993) 287–291.

[56] Yonatan Kahn, Gordan Krnjaic, Jesse Thaler, and Matthew Toups, “*DAE δ ALUS and dark matter detection*,” *Phys. Rev. D* **91** no. 5, (2015) 055006, [[arXiv:1411.1055](https://arxiv.org/abs/1411.1055) [hep-ph]].

[57] Brian Batell, Rouven Essig, and Ze’ev Surujon, “*Strong Constraints on Sub-GeV Dark Sectors from SLAC Beam Dump E137*,” *Phys. Rev. Lett.* **113** no. 17, (2014) 171802, [[arXiv:1406.2698](https://arxiv.org/abs/1406.2698) [hep-ph]].

[58] Asher Berlin, Nikita Blinov, Gordan Krnjaic, Philip Schuster, and Natalia Toro, “*Dark Matter, Millicharges, Axion and Scalar Particles, Gauge Bosons, and Other New Physics with LDMX*,” *Phys. Rev. D* **99** no. 7, (2019) 075001, [[arXiv:1807.01730](https://arxiv.org/abs/1807.01730) [hep-ph]].

[59] D. Banerjee et al., “*Dark matter search in missing energy events with NA64*,” *Phys. Rev. Lett.* **123** no. 12, (2019) 121801, [[arXiv:1906.00176](https://arxiv.org/abs/1906.00176) [hep-ex]].

[60] Bhaskar Dutta, Doojin Kim, Shu Liao, Jong-Chul Park, Seodong Shin, and Louis E. Strigari, “*Dark matter signals from timing spectra at neutrino experiments*,” *Phys. Rev. Lett.* **124** no. 12, (2020) 121802, [[arXiv:1906.10745](https://arxiv.org/abs/1906.10745) [hep-ph]].

[61] Asher Berlin, Patrick deNiverville, Adam Ritz, Philip Schuster, and Natalia Toro, “*Sub-GeV dark matter production at fixed-target experiments*,” *Phys. Rev. D* **102** no. 9, (2020) 095011, [[arXiv:2003.03379](https://arxiv.org/abs/2003.03379) [hep-ph]].

[62] Nikita Blinov, Gordan Krnjaic, and Douglas Tuckler, “*Characterizing Dark Matter Signals with Missing Momentum Experiments*,” *Phys. Rev. D* **103** no. 3, (2021) 035030, [[arXiv:2010.03577](https://arxiv.org/abs/2010.03577) [hep-ph]].

[63] Marco Costa, Rashmish K. Mishra, and Sonali Verma, “*Model agnostic probes of dark sectors at neutrino experiments*,” *Phys. Rev. D* **108** no. 3, (2023) 035041, [[arXiv:2211.13253](https://arxiv.org/abs/2211.13253) [hep-ph]].

[64] Alexey S. Zhevlakov, Dmitry V. Kirpichnikov, and Valery E. Lyubovitskij, “*Implication of the dark axion portal for the EDM of fermions and dark matter probing with NA64e, NA64 μ , LDMX, M3, and BaBar*,” *Phys. Rev. D* **106** no. 3, (2022) 035018, [[arXiv:2204.09978](https://arxiv.org/abs/2204.09978) [hep-ph]].

[65] Asli M. Abdullahi, Matheus Hostert, Daniele Massaro, and Silvia Pascoli, “*Semi-Visible Dark Photon Phenomenology at the GeV Scale*,” *Phys. Rev. D* **108** no. 1, (2023) 015032, [[arXiv:2302.05410](https://arxiv.org/abs/2302.05410) [hep-ph]].

[66] Sergei N. Gninenko, Dmitry V. Kirpichnikov, Sergey Kuleshov, Valery E. Lyubovitskij, and Alexey S. Zhevlakov, “*Test of the vector portal with dark fermions in the charge-exchange reactions in the NA64 experiment at CERN SPS*,” *Phys. Rev. D* **109** no. 7, (2024) 075021, [[arXiv:2312.01703](https://arxiv.org/abs/2312.01703) [hep-ph]].

[67] Chuan-Hung Chen, Chao-Qiang Geng, and Tzu-Chiang Yuan, “*Non-standard neutrino interactions in $K^+ \rightarrow \pi^+ \nu \bar{\nu}$ and $D^+ \rightarrow \pi^+ \nu \bar{\nu}$ decays*,” *Phys. Rev. D* **75** (2007) 077301, [[arXiv:hep-ph/0703196](https://arxiv.org/abs/hep-ph/0703196)].

[68] Jernej F. Kamenik and Christopher Smith, “*FCNC portals to the dark sector*,” *JHEP* **03** (2012) 090, [[arXiv:1111.6402](https://arxiv.org/abs/1111.6402) [hep-ph]].

[69] Ze-Kun Liu, Ying Li, Biao-Feng Hou, and Qin Chang, “*Search for Light Dark Matter in Rare Meson Decays*,” [[arXiv:2512.21191](https://arxiv.org/abs/2512.21191) [hep-ph]].

[70] Federico Mescia, Shohei Okawa, Joel Swallow, and Claudio Toni, “*Dark Matter emission at Belle II and NA62 in Minimal Flavor Violation framework*,” [[arXiv:2601.08907](https://arxiv.org/abs/2601.08907) [hep-ph]].

[71] Brian Batell, Ayres Freitas, Ahmed Ismail, and David McKeen, “*Probing Light Dark Matter with a Hadrophilic Scalar Mediator*,” *Phys. Rev. D* **100** no. 9, (2019) 095020, [[arXiv:1812.05103](https://arxiv.org/abs/1812.05103) [hep-ph]].

[72] James Alvey, Miguel Campos, Malcolm Fairbairn, and Tevong You, “*Detecting Light Dark Matter via Inelastic Cosmic Ray Collisions*,” *Phys. Rev. Lett.* **123** (2019) 261802, [[arXiv:1905.05776](https://arxiv.org/abs/1905.05776) [hep-ph]].

[73] Victor V. Flambaum, Liangliang Su, Lei Wu, and Bin Zhu, “*New strong bounds on sub-GeV dark matter from boosted and Migdal effects*,” *Sci. China Phys. Mech. Astron.* **66** no. 7, (2023) 271011, [[arXiv:2012.09751](https://arxiv.org/abs/2012.09751) [hep-ph]].

[74] Liangliang Su, Lei Wu, Ning Zhou, and Bin Zhu, “*Accelerated-light-dark-matter-Earth inelastic scattering in direct detection*,” *Phys. Rev. D* **108** no. 3, (2023) 035004, [[arXiv:2212.02286](https://arxiv.org/abs/2212.02286) [hep-ph]].

[75] **PandaX** Collaboration, Xuyang Ning et al., “*Search for Light Dark Matter from the Atmosphere in PandaX-4T*,” *Phys. Rev. Lett.* **131** no. 4, (2023) 041001, [[arXiv:2301.03010](https://arxiv.org/abs/2301.03010) [hep-ex]].

[76] **BESIII** Collaboration, Medina Ablikim et al., “*Search for sub-GeV dark particles in $\eta \rightarrow \pi^0 + \text{invisible decay}$* ,” [[arXiv:2601.10597](https://arxiv.org/abs/2601.10597) [hep-ex]].

[77] Jeff A. Dror, Gilly Elor, and Robert Mcgehee, “*Absorption of Fermionic Dark Matter by Nuclear Targets*,” *JHEP* **02** (2020) 134, [[arXiv:1908.10861](https://arxiv.org/abs/1908.10861) [hep-ph]].

[78] Nicholas Hurtado, Hana Mir, Ian M. Shoemaker, Eli Welch, and Jason Wyenberg, “*Dark Matter-Neutrino Interconversion at COHERENT, Direct Detection, and the Early Universe*,” *Phys. Rev. D* **102** no. 1, (2020) 015006, [[arXiv:2005.13384](https://arxiv.org/abs/2005.13384) [hep-ph]].

[79] Gang Li, Chuan-Qiang Song, Feng-Jie Tang, and Jiang-Hao Yu, “*A Comprehensive Effective Field Theory Framework for Coherent Elastic Neutrino-Nucleus Scattering*,” [[arXiv:2601.19883](https://arxiv.org/abs/2601.19883) [hep-ph]].

[80] Pablo M. Candela, Valentina De Romeri, and Dimitrios K. Papoulias, “*COHERENT production of a dark fermion*,” *Phys. Rev. D* **108** no. 5, (2023) 055001, [[arXiv:2305.03341](https://arxiv.org/abs/2305.03341) [hep-ph]].

[81] Yugen Lin, Chih-Ting Lu, and Ningqiang Song, “*Supernova cooling from neutrino-devouring dark matter*,” [[arXiv:2507.22124](https://arxiv.org/abs/2507.22124) [hep-ph]].

[82] Peter Minkowski, “ $\mu \rightarrow e\gamma$ at a Rate of One Out of 10^9 Muon Decays?,” *Phys. Lett. B* **67** (1977) 421–428.

[83] Rabindra N. Mohapatra and Goran Senjanovic, “*Neutrino Mass and Spontaneous Parity Nonconservation*,” *Phys. Rev. Lett.* **44** (1980) 912.

[84] Tsutomu Yanagida, “*Horizontal gauge symmetry and masses of neutrinos*,” *Conf. Proc. C* **7902131** (1979) 95–99.

[85] Murray Gell-Mann, Pierre Ramond, and Richard Slansky, “*Complex Spinors and Unified Theories*,” *Conf. Proc. C* **790927** (1979) 315–321, [[arXiv:1306.4669](https://arxiv.org/abs/1306.4669) [hep-th]].

[86] S. L. Glashow, “*The Future of Elementary Particle Physics*,” *NATO Sci. Ser. B* **61** (1980) 687.

[87] Vedran Brdar, Werner Rodejohann, and Xun-Jie Xu, “*Producing a new Fermion in Coherent Elastic Neutrino-Nucleus Scattering: from Neutrino Mass to Dark Matter*,” *JHEP* **12** (2018) 024, [[arXiv:1810.03626](https://arxiv.org/abs/1810.03626) [hep-ph]].

[88] Wei Chao, Tong Li, Jiajun Liao, and Min Su, “*Loop effects with a vector mediator in coherent neutrino-nucleus scattering*,” *Phys. Rev. D* **104** no. 9, (2021) 095017, [[arXiv:2108.02341](https://arxiv.org/abs/2108.02341) [hep-ph]].

[89] Pablo M. Candela, Valentina De Romeri, Pantelis Melas, Dimitrios K. Papoulias, and Niki Saoulidou, “*Up-scattering production of a sterile fermion at DUNE: complementarity with spallation source and direct detection experiments*,” *JHEP* **10** (2024) 032, [[arXiv:2404.12476](https://arxiv.org/abs/2404.12476) [hep-ph]].

[90] T. S. Kosmas, D. K. Papoulias, M. Tortola, and J. W. F. Valle, “*Probing light sterile neutrino signatures at reactor and Spallation Neutron Source neutrino experiments*,” *Phys. Rev. D* **96** no. 6, (2017) 063013, [[arXiv:1703.00054](https://arxiv.org/abs/1703.00054) [hep-ph]].

[91] Carlos Blanco, Dan Hooper, and Pedro Machado, “*Constraining Sterile Neutrino Interpretations of the LSND and MiniBooNE Anomalies with Coherent Neutrino Scattering Experiments*,” *Phys. Rev. D* **101** no. 7, (2020) 075051, [[arXiv:1901.08094](https://arxiv.org/abs/1901.08094) [hep-ph]].

[92] Jeffrey M. Berryman, “*Constraining Sterile Neutrino Cosmology with Terrestrial Oscillation Experiments*,” *Phys. Rev. D* **100** no. 2, (2019) 023540, [[arXiv:1905.03254](https://arxiv.org/abs/1905.03254) [hep-ph]].

[93] O. G. Miranda, D. K. Papoulias, O. Sanders, M. Tórtola, and J. W. F. Valle, “*Future CEvNS experiments as probes of lepton unitarity and light-sterile neutrinos*,” *Phys. Rev. D* **102** (2020) 113014, [[arXiv:2008.02759](https://arxiv.org/abs/2008.02759) [hep-ph]].

[94] D. Alonso-González, D. W. P. Amaral, A. Bariego-Quintana, D. Cerdeño, and M. de los Rios, “*Measuring the sterile neutrino mass in spallation source and direct detection experiments*,” *JHEP* **12** (2023) 096, [[arXiv:2307.05176](https://arxiv.org/abs/2307.05176) [hep-ph]].

[95] S. P. Behera, D. K. Mishra, P. K. Netrakanti, R. Sehgal, Kirtikesh Kumar, R. Dey, and V. Jha, “*Sterile neutrino searches with reactor antineutrinos using coherent neutrino-nucleus scattering experiments*,” *Phys. Rev. D* **108** no. 11, (2023) 113002, [[arXiv:2304.00912](https://arxiv.org/abs/2304.00912) [hep-ph]].

[96] Patrick D. Bolton, Frank F. Deppisch, and P. S. Bhupal Dev, “*Neutrinoless double beta decay versus other probes of heavy sterile neutrinos*,” *JHEP* **03** (2020) 170, [[arXiv:1912.03058](https://arxiv.org/abs/1912.03058) [hep-ph]].

[97] <https://www.hep.ucl.ac.uk/~pbolton/>.

[98] P. Vogel and J. Engel, “*Neutrino Electromagnetic Form-Factors*,” *Phys. Rev. D* **39** (1989) 3378.

[99] A. B. Balantekin and N. Vassh, “*Magnetic moments of active and sterile neutrinos*,” *Phys. Rev. D* **89** no. 7, (2014) 073013, [[arXiv:1312.6858](https://arxiv.org/abs/1312.6858) [hep-ph]].

[100] Gabriel Magill, Ryan Plestid, Maxim Pospelov, and Yu-Dai Tsai, “*Dipole Portal to Heavy Neutral Leptons*,” *Phys. Rev. D* **98** no. 11, (2018) 115015, [[arXiv:1803.03262](https://arxiv.org/abs/1803.03262) [hep-ph]].

[101] Ian M. Shoemaker and Jason Wyenberg, “*Direct Detection Experiments at the Neutrino Dipole Portal Frontier*,” *Phys. Rev. D* **99** no. 7, (2019) 075010, [[arXiv:1811.12435](https://arxiv.org/abs/1811.12435) [hep-ph]].

[102] Vedran Brdar, Admir Greljo, Joachim Kopp, and Toby Opferkuch, “*The Neutrino Magnetic Moment Portal: Cosmology, Astrophysics, and Direct Detection*,” *JCAP* **01** (2021) 039, [[arXiv:2007.15563](https://arxiv.org/abs/2007.15563) [hep-ph]].

[103] Thomas Schwetz, Albert Zhou, and Jing-Yu Zhu, “*Constraining active-sterile neutrino transition magnetic moments at DUNE near and far detectors*,” *JHEP* **21** (2020) 200, [[arXiv:2105.09699](https://arxiv.org/abs/2105.09699) [hep-ph]].

[104] Ian M. Shoemaker, Yu-Dai Tsai, and Jason Wyenberg, “*Active-to-sterile neutrino dipole portal and the XENON1T excess*,” *Phys. Rev. D* **104** no. 11, (2021) 115026, [[arXiv:2007.05513](https://arxiv.org/abs/2007.05513) [hep-ph]].

[105] Mack Atkinson, Pilar Coloma, Ivan Martinez-Soler, Noemi Rocco, and Ian M. Shoemaker, “*Heavy Neutrino Searches through Double-Bang Events at Super-Kamiokande, DUNE, and Hyper-Kamiokande*,” *JHEP* **04** (2022) 174, [[arXiv:2105.09357](https://arxiv.org/abs/2105.09357) [hep-ph]].

[106] O. G. Miranda, D. K. Papoulias, O. Sanders, M. Tórtola, and J. W. F. Valle, “*Low-energy probes of sterile neutrino transition magnetic moments*,” *JHEP* **12** (2021) 191, [[arXiv:2109.09545](https://arxiv.org/abs/2109.09545) [hep-ph]].

[107] Patrick D. Bolton, Frank F. Deppisch, Kåre Fridell, Julia Harz, Chandan Hati, and Suchita Kulkarni, “*Probing active-sterile neutrino transition magnetic moments with photon emission from CEvNS*,” *Phys. Rev. D* **106** no. 3, (2022) 035036, [[arXiv:2110.02233](https://arxiv.org/abs/2110.02233) [hep-ph]].

[108] V. De Romeri, O. G. Miranda, D. K. Papoulias, G. Sanchez Garcia, M. Tórtola, and J. W. F. Valle, “*Physics implications of a combined analysis of COHERENT CsI and LAr data*,” *JHEP* **04** (2023) 035, [[arXiv:2211.11905](https://arxiv.org/abs/2211.11905) [hep-ph]].

[109] Maksym Ovchynnikov, Thomas Schwetz, and Jing-Yu Zhu, “*Dipole portal and neutrinoophilic scalars at DUNE revisited: The importance of the high-energy neutrino tail*,” *Phys. Rev. D* **107** no. 5, (2023) 055029, [[arXiv:2210.13141](https://arxiv.org/abs/2210.13141) [hep-ph]].

[110] **FCC** Collaboration, A. Abada et al., “*FCC-ee: The Lepton Collider: Future Circular Collider Conceptual Design Report Volume 2*,” *Eur. Phys. J. ST* **228** no. 2, (2019) 261–623.

[111] **CEPC Study Group** Collaboration, Mingyi Dong et al., “*CEPC Conceptual Design Report: Volume 2 - Physics & Detector*,” [[arXiv:1811.10545](https://arxiv.org/abs/1811.10545) [hep-ex]].

[112] **ILC** Collaboration, “*The International Linear Collider Technical Design Report - Volume 2: Physics*,” [[arXiv:1306.6352](https://arxiv.org/abs/1306.6352) [hep-ph]].

[113] Philip Bambade et al., “*The International Linear Collider: A Global Project*,” [[arXiv:1903.01629](https://arxiv.org/abs/1903.01629) [hep-ex]].

[114] **CLIC accelerator** Collaboration, “*The Compact Linear Collider (CLIC) - Project Implementation Plan*,” [[arXiv:1903.08655](https://arxiv.org/abs/1903.08655) [physics.acc-ph]].

[115] Rebeca Beltrán, Giovanna Cottin, Juan Carlos Helo, Martin Hirsch, Arsenii Titov, and Zeren Simon Wang, “*Long-lived heavy neutral leptons at the LHC: four-fermion single- N_R operators*,” *JHEP* **01** (2022) 044, [[arXiv:2110.15096](https://arxiv.org/abs/2110.15096) [hep-ph]].

[116] Manimala Mitra, Sanjoy Mandal, Rojalin Padhan, Agnivo Sarkar, and Michael Spannowsky, “*Reexamining right-handed neutrino EFTs up to dimension six*,” *Phys. Rev. D* **106** no. 11, (2022) 113008, [[arXiv:2210.12404](https://arxiv.org/abs/2210.12404) [hep-ph]].

[117] Mikhail A. Shifman, A. I. Vainshtein, and Valentin I. Zakharov, “*Remarks on Higgs Boson Interactions with Nucleons*,” *Phys. Lett. B* **78** (1978) 443–446.

[118] Manuel Drees and Mihoko Nojiri, “*Neutralino - nucleon scattering revisited*,” *Phys. Rev. D* **48** (1993) 3483–3501, [[arXiv:hep-ph/9307208](https://arxiv.org/abs/hep-ph/9307208)].

[119] Andreas Crivellin, Martin Hoferichter, and Massimiliano Procura, “*Accurate evaluation of hadronic uncertainties in spin-independent WIMP-nucleon scattering: Disentangling two- and three-flavor effects*,” *Phys. Rev. D* **89** (2014) 054021, [[arXiv:1312.4951](https://arxiv.org/abs/1312.4951) [hep-ph]].

[120] Fady Bishara, Joachim Brod, Benjamin Grinstein, and Jure Zupan, “*From quarks to nucleons in dark matter direct detection*,” *JHEP* **11** (2017) 059, [[arXiv:1707.06998](https://arxiv.org/abs/1707.06998) [hep-ph]].

[121] Junji Hisano, Koji Ishiwata, and Natsumi Nagata, “*A complete calculation for direct detection of Wino dark matter*,” *Phys. Lett. B* **690** (2010) 311–315, [[arXiv:1004.4090](https://arxiv.org/abs/1004.4090) [hep-ph]].

[122] Junji Hisano, Koji Ishiwata, and Natsumi Nagata, “*Gluon contribution to the dark matter direct detection*,” *Phys. Rev. D* **82** (2010) 115007, [[arXiv:1007.2601](https://arxiv.org/abs/1007.2601) [hep-ph]].

[123] Junji Hisano, Koji Ishiwata, Natsumi Nagata, and Tomohiro Takesako, “*Direct Detection of Electroweak-Interacting Dark Matter*,” *JHEP* **07** (2011) 005, [[arXiv:1104.0228](https://arxiv.org/abs/1104.0228) [hep-ph]].

[124] Richard J. Hill and Mikhail P. Solon, “*Universal behavior in the scattering of heavy, weakly interacting dark matter on nuclear targets*,” *Phys. Lett. B* **707** (2012) 539–545, [[arXiv:1111.0016](https://arxiv.org/abs/1111.0016) [hep-ph]].

[125] Richard J. Hill and Mikhail P. Solon, “*Standard Model anatomy of WIMP dark matter direct detection I: weak-scale matching*,” *Phys. Rev. D* **91** (2015) 043504, [[arXiv:1401.3339](https://arxiv.org/abs/1401.3339) [hep-ph]].

[126] Alejandro Ibarra and Sebastian Wild, “*Dirac dark matter with a charged mediator: a comprehensive one-loop analysis of the direct detection phenomenology*,” *JCAP* **05** (2015) 047, [[arXiv:1503.03382](https://arxiv.org/abs/1503.03382) [hep-ph]].

[127] Tomohiro Abe and Ryosuke Sato, “*Quantum corrections to the spin-independent cross section of the inert doublet dark matter*,” *JHEP* **03** (2015) 109, [[arXiv:1501.04161](https://arxiv.org/abs/1501.04161) [hep-ph]].

[128] Tomohiro Abe, Motoko Fujiwara, and Junji Hisano, “*Loop corrections to dark matter direct detection in a pseudoscalar mediator dark matter model*,” *JHEP* **02** (2019) 028, [[arXiv:1810.01039](https://arxiv.org/abs/1810.01039) [hep-ph]].

[129] Fatih Ertas and Felix Kahlhoefer, “*Loop-induced direct detection signatures from CP-violating scalar mediators*,” *JHEP* **06** (2019) 052, [[arXiv:1902.11070](https://arxiv.org/abs/1902.11070) [hep-ph]].

[130] **COHERENT** Collaboration, D. Akimov et al., “*The COHERENT Experiment at the Spallation Neutron Source*,” [[arXiv:1509.08702](https://arxiv.org/abs/1509.08702) [physics.ins-det]].

[131] **CONUS+** Collaboration, N. Ackermann et al., “*CONUS+ Experiment*,” *Eur. Phys. J. C* **84** no. 12, (2024) 1265, [[arXiv:2407.11912](https://arxiv.org/abs/2407.11912) [hep-ex]]. [Erratum: *Eur.Phys.J.C* 85, 19 (2025)].

[132] **DUNE** Collaboration, R. Acciari et al., “*Long-Baseline Neutrino Facility (LBNF) and Deep Underground Neutrino Experiment (DUNE): Conceptual Design Report, Volume 2: The Physics Program for DUNE at LBNF*,” [[arXiv:1512.06148](https://arxiv.org/abs/1512.06148) [physics.ins-det]].

[133] Jonathan L. Feng, Jason Kumar, Danny Marfatia, and David Sanford, “*Isospin-Violating Dark Matter*,” *Phys. Lett. B* **703** (2011) 124–127, [[arXiv:1102.4331](https://arxiv.org/abs/1102.4331) [hep-ph]].

[134] Daniel Z. Freedman, “*Coherent Neutrino Nucleus Scattering as a Probe of the Weak Neutral Current*,” *Phys. Rev. D* **9** (1974) 1389–1392.

[135] **COHERENT** Collaboration, D. Akimov et al., “*Measurement of the Coherent Elastic Neutrino-Nucleus Scattering Cross Section on CsI by COHERENT*,” *Phys. Rev. Lett.* **129** no. 8, (2022) 081801, [[arXiv:2110.07730](https://arxiv.org/abs/2110.07730) [hep-ex]].

[136] **COHERENT** Collaboration, D. Akimov et al., “*Observation of Coherent Elastic Neutrino-Nucleus Scattering*,” *Science* **357** no. 6356, (2017) 1123–1126, [[arXiv:1708.01294](https://arxiv.org/abs/1708.01294) [nucl-ex]].

[137] W. C. Louis, “*Searches for muon-to-electron (anti) neutrino flavor change*,” *Prog. Part. Nucl. Phys.* **63** (2009) 51–73.

[138] A. Drukier and Leo Stodolsky, “*Principles and Applications of a Neutral Current Detector for Neutrino Physics and Astronomy*,” *Phys. Rev. D* **30** (1984) 2295.

[139] N. Ackermann et al., “*Direct observation of coherent elastic antineutrino–nucleus scattering*,” *Nature* **643** no. 8074, (2025) 1229–1233, [[arXiv:2501.05206](https://arxiv.org/abs/2501.05206) [hep-ex]].

[140] Ayan Chattaraj, Anirban Majumdar, and Rahul Srivastava, “*Probing standard model and beyond with reactor CEνNS data of CONUS+ experiment*,” *Phys. Lett. B* **864** (2025) 139438, [[arXiv:2501.12441](https://arxiv.org/abs/2501.12441) [hep-ph]].

[141] Valentina De Romeri, Dimitrios K. Papoulias, and Gonzalo Sanchez Garcia, “*Implications of the first CONUS+ measurement of coherent elastic neutrino-nucleus scattering*,” *Phys. Rev. D* **111** no. 7, (2025) 075025, [[arXiv:2501.17843](https://arxiv.org/abs/2501.17843) [hep-ph]].

[142] Manfred Lindner, Thomas Rink, and Manibrata Sen, “*Light vector bosons and the weak mixing angle in the light of future germanium-based reactor CEνNS experiments*,” *JHEP* **08** (2024) 171, [[arXiv:2401.13025](https://arxiv.org/abs/2401.13025) [hep-ph]].

[143] A. Bonhomme et al., “*Direct measurement of the ionization quenching factor of nuclear recoils in germanium in the keV energy range*,” *Eur. Phys. J. C* **82** no. 9, (2022) 815, [[arXiv:2202.03754](https://arxiv.org/abs/2202.03754) [physics.ins-det]].

[144] V. I. Kopeikin, “*Flux and spectrum of reactor antineutrinos*,” *Phys. Atom. Nucl.* **75** (2012) 143–152.

[145] Th. A. Mueller et al., “*Improved Predictions of Reactor Antineutrino Spectra*,” *Phys. Rev. C* **83** (2011) 054615, [[arXiv:1101.2663](https://arxiv.org/abs/1101.2663) [hep-ex]].

[146] **DUNE** Collaboration, V. Hewes et al., “*Deep Underground Neutrino Experiment (DUNE) Near Detector Conceptual Design Report*,” *Instruments* **5** no. 4, (2021) 31, [[arXiv:2103.13910](https://arxiv.org/abs/2103.13910) [physics.ins-det]].

[147] L. Fields. <https://home.fnal.gov/~ljf26/DUNEfluxes/>.

[148] <https://glaucus.crc.nd.edu/DUNEfluxes/>.

[149] Varun Mathur, Ian M. Shoemaker, and Zahra Tabrizi, “*Using DUNE to shed light on the electromagnetic properties of neutrinos*,” *JHEP* **10** (2022) 041, [[arXiv:2111.14884](https://arxiv.org/abs/2111.14884) [hep-ph]].

[150] **DUNE** Collaboration, R. Acciarri et al., “*Long-Baseline Neutrino Facility (LBNF) and Deep Underground Neutrino Experiment (DUNE): Conceptual Design Report, Volume 1: The LBNF and DUNE Projects*,” [[arXiv:1601.05471](https://arxiv.org/abs/1601.05471) [physics.ins-det]].

[151] Peter Ballett, Tommaso Boschi, and Silvia Pascoli, “*Heavy Neutral Leptons from low-scale seesaws at the DUNE Near Detector*,” *JHEP* **03** (2020) 111, [[arXiv:1905.00284](https://arxiv.org/abs/1905.00284) [hep-ph]].

[152] **DUNE** Collaboration, T. Alion et al., “*Experiment Simulation Configurations Used in DUNE CDR*,” [[arXiv:1606.09550](https://arxiv.org/abs/1606.09550) [physics.ins-det]].

[153] Valentina De Romeri, Kevin J. Kelly, and Pedro A. N. Machado, “*DUNE-PRISM Sensitivity to Light Dark Matter*,” *Phys. Rev. D* **100** no. 9, (2019) 095010, [[arXiv:1903.10505](https://arxiv.org/abs/1903.10505) [hep-ph]].

[154] Pantelis Melas, Dimitrios K. Papoulias, and Niki Saoulidou, “*Probing generalized neutrino interactions with the DUNE Near Detector*,” *JHEP* **07** (2023) 190, [[arXiv:2303.07094](https://arxiv.org/abs/2303.07094) [hep-ph]].

[155] Andre de Gouvea, Pedro A. N. Machado, Yuber F. Perez-Gonzalez, and Zahra Tabrizi, “*Measuring the Weak Mixing Angle in the DUNE Near Detector Complex*,” *Phys. Rev. Lett.* **125** no. 5, (2020) 051803, [[arXiv:1912.06658](https://arxiv.org/abs/1912.06658) [hep-ph]].

[156] P. S. Bhupal Dev, Doojin Kim, Kuver Sinha, and Yongchao Zhang, “*New interference effects from light gauge bosons in neutrino-electron scattering*,” *Phys. Rev. D* **104** no. 7, (2021) 075001, [[arXiv:2105.09309](https://arxiv.org/abs/2105.09309) [hep-ph]].

[157] **ATLAS** Collaboration, Georges Aad et al., “*Search for new phenomena in events with an*

energetic jet and missing transverse momentum in pp collisions at $\sqrt{s} = 13$ TeV with the ATLAS detector,” *Phys. Rev. D* **103** no. 11, (2021) 112006, [[arXiv:2102.10874](https://arxiv.org/abs/2102.10874) [hep-ex]].

[158] **CMS** Collaboration, Armen Tumasyan et al., “*Search for new particles in events with energetic jets and large missing transverse momentum in proton-proton collisions at $\sqrt{s} = 13$ TeV,”* *JHEP* **11** (2021) 153, [[arXiv:2107.13021](https://arxiv.org/abs/2107.13021) [hep-ex]].

[159] **ATLAS** Collaboration, Georges Aad et al., “*Search for dark matter in association with an energetic photon in pp collisions at $\sqrt{s} = 13$ TeV with the ATLAS detector,”* *JHEP* **02** (2021) 226, [[arXiv:2011.05259](https://arxiv.org/abs/2011.05259) [hep-ex]].

[160] **ATLAS** Collaboration, Georges Aad et al., “*Search for associated production of a Z boson with an invisibly decaying Higgs boson or dark matter candidates at $s=13$ TeV with the ATLAS detector,”* *Phys. Lett. B* **829** (2022) 137066, [[arXiv:2111.08372](https://arxiv.org/abs/2111.08372) [hep-ex]].

[161] **ATLAS** Collaboration, M. Aaboud et al., “*Search for dark matter in events with a hadronically decaying vector boson and missing transverse momentum in pp collisions at $\sqrt{s} = 13$ TeV with the ATLAS detector,”* *JHEP* **10** (2018) 180, [[arXiv:1807.11471](https://arxiv.org/abs/1807.11471) [hep-ex]].

[162] **ATLAS** Collaboration, Georges Aad et al., “*Search for new particles in events with a hadronically decaying W or Z boson and large missing transverse momentum at $\sqrt{s} = 13$ TeV using the ATLAS detector,”* *JHEP* **11** (2024) 126, [[arXiv:2406.01272](https://arxiv.org/abs/2406.01272) [hep-ex]].

[163] G. G. Raffelt, Stars as laboratories for fundamental physics: The astrophysics of neutrinos, axions, and other weakly interacting particles. 5, 1996.

[164] **PandaX** Collaboration, Linhui Gu et al., “*First Search for the Absorption of Fermionic Dark Matter with the PandaX-4T Experiment,”* *Phys. Rev. Lett.* **129** no. 16, (2022) 161803, [[arXiv:2205.15771](https://arxiv.org/abs/2205.15771) [hep-ex]].

[165] **Majorana** Collaboration, I. J. Arnquist et al., “*Exotic Dark Matter Search with the Majorana Demonstrator,”* *Phys. Rev. Lett.* **132** no. 4, (2024) 041001, [[arXiv:2206.10638](https://arxiv.org/abs/2206.10638) [hep-ex]].

[166] **CDEX** Collaboration, W. H. Dai et al., “*Exotic Dark Matter Search with the CDEX-10 Experiment at China’s Jinping Underground Laboratory,”* *Phys. Rev. Lett.* **129** no. 22, (2022) 221802, [[arXiv:2209.00861](https://arxiv.org/abs/2209.00861) [hep-ex]].

[167] **PICO** Collaboration, E. Adams et al., “*Absorption of Fermionic Dark Matter in the PICO-60 C3F8 Bubble Chamber,”* *Phys. Rev. Lett.* **135** no. 1, (2025) 011001, [[arXiv:2504.13089](https://arxiv.org/abs/2504.13089) [hep-ex]].

[168] Brian Batell, Jonathan L. Feng, Ahmed Ismail, Felix Kling, Roshan Mammen Abraham, and Sebastian Trojanowski, “*Discovering dark matter at the LHC through its nuclear scattering in far-forward emulsion and liquid argon detectors,”* *Phys. Rev. D* **104** no. 3, (2021) 035036, [[arXiv:2107.00666](https://arxiv.org/abs/2107.00666) [hep-ph]].

[169] Brian Batell, Jonathan L. Feng, and Sebastian Trojanowski, “*Detecting Dark Matter with Far-Forward Emulsion and Liquid Argon Detectors at the LHC,”* *Phys. Rev. D* **103** no. 7, (2021) 075023, [[arXiv:2101.10338](https://arxiv.org/abs/2101.10338) [hep-ph]].

[170] Patrick deNiverville, David McKeen, and Adam Ritz, “*Signatures of sub-GeV dark matter beams at neutrino experiments,”* *Phys. Rev. D* **86** (2012) 035022, [[arXiv:1205.3499](https://arxiv.org/abs/1205.3499) [hep-ph]].

[171] Miriam D. Diamond and Philip Schuster, “*Searching for Light Dark Matter with the SLAC Millicharge Experiment*,” *Phys. Rev. Lett.* **111** no. 22, (2013) 221803, [[arXiv:1307.6861](https://arxiv.org/abs/1307.6861) [hep-ph]].

[172] Eder Izaguirre, Gordan Krnjaic, Philip Schuster, and Natalia Toro, “*New Electron Beam-Dump Experiments to Search for MeV to few-GeV Dark Matter*,” *Phys. Rev. D* **88** (2013) 114015, [[arXiv:1307.6554](https://arxiv.org/abs/1307.6554) [hep-ph]].

[173] Brian Batell, Patrick deNiverville, David McKeen, Maxim Pospelov, and Adam Ritz, “*Leptophobic Dark Matter at Neutrino Factories*,” *Phys. Rev. D* **90** no. 11, (2014) 115014, [[arXiv:1405.7049](https://arxiv.org/abs/1405.7049) [hep-ph]].

[174] **BaBar** Collaboration, J. P. Lees et al., “*Search for Invisible Decays of a Dark Photon Produced in e^+e^- Collisions at BaBar*,” *Phys. Rev. Lett.* **119** no. 13, (2017) 131804, [[arXiv:1702.03327](https://arxiv.org/abs/1702.03327) [hep-ex]].

[175] Brian Batell, Maxim Pospelov, and Adam Ritz, “*Exploring Portals to a Hidden Sector Through Fixed Targets*,” *Phys. Rev. D* **80** (2009) 095024, [[arXiv:0906.5614](https://arxiv.org/abs/0906.5614) [hep-ph]].

[176] Eder Izaguirre, Gordan Krnjaic, Philip Schuster, and Natalia Toro, “*Physics motivation for a pilot dark matter search at Jefferson Laboratory*,” *Phys. Rev. D* **90** no. 1, (2014) 014052, [[arXiv:1403.6826](https://arxiv.org/abs/1403.6826) [hep-ph]].

[177] Patrick deNiverville, Maxim Pospelov, and Adam Ritz, “*Observing a light dark matter beam with neutrino experiments*,” *Phys. Rev. D* **84** (2011) 075020, [[arXiv:1107.4580](https://arxiv.org/abs/1107.4580) [hep-ph]].

[178] Sowmiya Balan et al., “*Resonant or asymmetric: the status of sub-GeV dark matter*,” *JCAP* **01** (2025) 053, [[arXiv:2405.17548](https://arxiv.org/abs/2405.17548) [hep-ph]].

[179] Bhaskar Dutta, Doojin Kim, Shu Liao, Jong-Chul Park, Seodong Shin, Louis E. Strigari, and Adrian Thompson, “*Searching for dark matter signals in timing spectra at neutrino experiments*,” *JHEP* **01** (2022) 144, [[arXiv:2006.09386](https://arxiv.org/abs/2006.09386) [hep-ph]].

[180] Riccardo Catena and Taylor R. Gray, “*Spin-1 thermal targets for dark matter searches at beam dump and fixed target experiments*,” *JCAP* **11** (2023) 058, [[arXiv:2307.02207](https://arxiv.org/abs/2307.02207) [hep-ph]].

[181] Martina Mongillo, Asli Abdullahi, Benjamin Banto Oberhauser, Paolo Crivelli, Matheus Hostert, Daniele Massaro, Laura Molina Bueno, and Silvia Pascoli, “*Constraining light thermal inelastic dark matter with NA64*,” *Eur. Phys. J. C* **83** no. 5, (2023) 391, [[arXiv:2302.05414](https://arxiv.org/abs/2302.05414) [hep-ph]].

[182] David E. Morrissey and Andrew Paul Spray, “*New Limits on Light Hidden Sectors from Fixed-Target Experiments*,” *JHEP* **06** (2014) 083, [[arXiv:1402.4817](https://arxiv.org/abs/1402.4817) [hep-ph]].

[183] **Belle** Collaboration, Y. Jin et al., “*Observation of $\tau^- \rightarrow \pi^- \nu_\tau e^+ e^-$ and search for $\tau^- \rightarrow \pi^- \nu_\tau \mu^+ \mu^-$* ,” *Phys. Rev. D* **100** no. 7, (2019) 071101, [[arXiv:1908.09353](https://arxiv.org/abs/1908.09353) [hep-ex]].

[184] **SINDRUM** Collaboration, S. Egli et al., “*Measurement of the Decay $\pi^+ \rightarrow e^+ \nu_e e^+ e^-$ and Search for a Light Higgs Boson*,” *Phys. Lett. B* **222** (1989) 533–537.

[185] A. A. Pobladuev et al., “*Experimental study of the radiative decays $K+ \rightarrow mu+ nu e+ e-$ and $K+ \rightarrow e+ nu e+ e^-$* ,” *Phys. Rev. Lett.* **89** (2002) 061803, [[arXiv:hep-ex/0204006](https://arxiv.org/abs/hep-ex/0204006)].

[186] **PIENU** Collaboration, A. Aguilar-Arevalo et al., “*Search for the rare decays $\pi^+ \rightarrow \mu^+ \nu_\mu \nu \bar{\nu}$ and $\pi^+ \rightarrow e^+ \nu_e \nu \bar{\nu}$* ,” *Phys. Rev. D* **102** no. 1, (2020) 012001, [[arXiv:2006.00389](https://arxiv.org/abs/2006.00389) [hep-ex]].

[187] J. Heintze et al., “*A Measurement of the $K^+ \rightarrow e^+ \text{ Neutrino gamma Structure Decay}$,*” *Nucl. Phys. B* **149** (1979) 365–380.

[188] **SINDRUM** Collaboration, Wilhelm H. Bertl et al., “*Search for the Decay $\mu^+ \rightarrow e^+ e^+ e^-$,*” *Nucl. Phys. B* **260** (1985) 1–31.

[189] **CLEO** Collaboration, M. S. Alam et al., “*Tau decays into three charged leptons and two neutrinos,*” *Phys. Rev. Lett.* **76** (1996) 2637–2641.

[190] Gerrit Bickendorf and Manuel Drees, “*Constraints on light leptophilic dark matter mediators from decay experiments,*” *Eur. Phys. J. C* **82** no. 12, (2022) 1163, [[arXiv:2206.05038](https://arxiv.org/abs/2206.05038) [hep-ph]].

[191] André de Gouvêa, P. S. Bhupal Dev, Bhaskar Dutta, Tathagata Ghosh, Tao Han, and Yongchao Zhang, “*Leptonic Scalars at the LHC,*” *JHEP* **07** (2020) 142, [[arXiv:1910.01132](https://arxiv.org/abs/1910.01132) [hep-ph]].

[192] Vedran Brdar, Manfred Lindner, Stefan Vogl, and Xun-Jie Xu, “*Revisiting neutrino self-interaction constraints from Z and τ decays,*” *Phys. Rev. D* **101** no. 11, (2020) 115001, [[arXiv:2003.05339](https://arxiv.org/abs/2003.05339) [hep-ph]].

[193] **Particle Data Group** Collaboration, S. Navas et al., “*Review of particle physics,*” *Phys. Rev. D* **110** no. 3, (2024) 030001.

[194] P. S. Bhupal Dev, Doojin Kim, Deepak Sathyam, Kuver Sinha, and Yongchao Zhang, “*New laboratory constraints on neutrophilic mediators,*” *Phys. Lett. B* **868** (2025) 139765, [[arXiv:2407.12738](https://arxiv.org/abs/2407.12738) [hep-ph]].

[195] **PandaX** Collaboration, Dan Zhang et al., “*Search for Light Fermionic Dark Matter Absorption on Electrons in PandaX-4T,*” *Phys. Rev. Lett.* **129** no. 16, (2022) 161804, [[arXiv:2206.02339](https://arxiv.org/abs/2206.02339) [hep-ex]].

[196] **EXO-200** Collaboration, S. Al Kharusi et al., “*Search for MeV electron recoils from dark matter in EXO-200,*” *Phys. Rev. D* **107** no. 1, (2023) 012007, [[arXiv:2207.00897](https://arxiv.org/abs/2207.00897) [hep-ex]].

[197] **CDEX** Collaboration, J. X. Liu et al., “*First Search for Light Fermionic Dark Matter Absorption on Electrons Using Germanium Detector in CDEX-10 Experiment,*” [[arXiv:2404.09793](https://arxiv.org/abs/2404.09793) [hep-ex]].

[198] Spencer Klein and Joakim Nystrand, “*Exclusive vector meson production in relativistic heavy ion collisions,*” *Phys. Rev. C* **60** (1999) 014903, [[arXiv:hep-ph/9902259](https://arxiv.org/abs/hep-ph/9902259)].

[199] Valentina De Romeri, Dimitrios K. Papoulias, Gonzalo Sanchez Garcia, Christoph A. Ternes, and Mariam Tórtola, “*Neutrino electromagnetic properties and sterile dipole portal in light of the first solar CE ν NS data,*” *JCAP* **05** (2025) 080, [[arXiv:2412.14991](https://arxiv.org/abs/2412.14991) [hep-ph]].

[200] Martin Hoferichter, Javier Menéndez, and Achim Schwenk, “*Coherent elastic neutrino-nucleus scattering: EFT analysis and nuclear responses,*” *Phys. Rev. D* **102** no. 7, (2020) 074018, [[arXiv:2007.08529](https://arxiv.org/abs/2007.08529) [hep-ph]].

[201] T. S. Kosmas, V. K. B. Kota, D. K. Papoulias, and R. Sahu, “*Coherent elastic neutrino-nucleus scattering (CE ν NS) event rates for Ge, Zn, and Si detector materials,*” *Phys. Rev. C* **104** no. 6, (2021) 064618, [[arXiv:2111.08488](https://arxiv.org/abs/2111.08488) [nucl-th]].